DEVELOPING SELF-ASSEMBLING NANOCAGES WITH NATURALLY OCCURING BACTERIAL PEPTIDES

Submitted by

Charlotte Louise Dridge

To the University of Exeter as a thesis for the degree of Masters by Research in Biological Science, September 2014.

I certify that all material in this thesis which is not my own work has been identified and that no material has previously been submitted and approved for the award of a degree by this or any other University.

Charlotte Louise Dridge

Acknowledgements

I would like to thank Clive Butler for giving me the opportunity to start this work, and for all of his help, support and enthusiasm throughout the project. Thanks to all of those in the Biocat at the University of Exeter for lots of help, support and coffee. In particular I owe huge thanks to Paul James who helped me to find my feet in my first few months and was always there throughout the project to talk through a problem, big or small. Many thanks also to Lizzy Dridge for being a great sister, friend and scientist and for knowing all of the answers to my questions.

I would also like to thank NanoSight Ltd for funding this work, in particular Bob Carr and Matthew Wright for being so accommodating on my trips to NanoSight and for the use of their equipment, a crucial part of this project.

Finally, thank you very much to my parents for their support, both financial and emotional. I cannot thank you enough for your love and generosity throughout these two years.

Abstract

The model selenate respiring bacterium *Thauera selenatis* produces selenium deposits on a nano-scale during selenate respiration. Selenium deposits have been isolated from *Thauera selenatis* growth medium, analysed and found to be red solid particles with a diameter of approximately 130 nm. Analysis of the growth medium has suggested that selenium deposits are exported out of the cell, in a process that is facilitated by a key protein termed the selenium export factor, SefA. This protein has been expressed in *Escherichia coli* and the two recombinant His-tagged forms (His-SefA and His-SefA-His) have been purified. It has been suggested that proteins may influence selenium nanoparticle assembly. Debieux and co-workers investigated the size of selenium nanospheres produced *in vitro* in the presence of His-SefA and found that they were approximately 300 nm in diameter. This is significantly different to those produced during the growth of *Thauera selenatis*, and so the effect of His-tagging the SefA protein on the selenium nanoparticles produced was investigated.

A non-His-tagged construct of the SefA protein, rSefA, was produced by proteolytic cleavage of the N-terminal His-tag from His-SefA using thrombin. This resulting protein with no His-tags was expected to produce selenium nanospheres most similar to those produced in *Thauera selenatis* during selenate respiration. Nanoparticles of approximately 130 nm in size, similar to those produced in the bacterium, were produced in the presence of 10 μg/ml rSefA. The size of the nanoparticles was determined using Nanoparticle Tracking Analysis in collaboration with NanoSight Ltd. Selenium nanospheres produced in the presence of His-SefA showed a decrease in particle size as the protein concentration increased. By contrast, those produced in the presence of rSefA showed an increase in particle size as the protein concentration increased. In the presence of His-SefA-His changing the protein concentration had no effect on the size of the selenium particles produced.

Abbreviations

BSA	Bovine serum albumin
CAPS	N-cyclohexyl-3-aminopropanesulphonic acid
E. coli	*Escherichia coli*
EDTA	Ethylenediaminetetraacetic acid
GS-Se-SG	Selenodiglutathione
GSH	Glutathione
HEPES	N-(2-Hydroxyethyl)piperazine-N'-(2-ethanesulphonic acid)
His-tag	Poly histidine tag
IPTG	Isopropyl-1-thio-β-D-galactopyranoside
LB	Lysogeny broth
MOPS	3-propanesulphonic acid
NTA	Nanoparticle tracking analysis
SDS	Sodium dodecyl sulphate
SefA	Selenium export factor A
T1SS	Type 1 secretion system
T6SS	Type 6 secretion system
TAT	Twin-arginine-translocation
TEM	Transmission electron microscopy
Tris-HCl	Tris (hydroxymethyl) aminomethane
T. selenatis	*Thauera selenatis*

Table of Contents

List of Figures

1 Introduction

1.1 An introduction to nanoparticles

The Encyclopaedia of Nanoscience and Nanotechnology defines a nanoparticle as a solid colloidal particle, which can range from 1 – 1000 nm in size (Soon-bark *et al.*, 2004). The colloidal particles consist of macromolecular materials that may include an active principle. This active principle may be encapsulated or dissolved in the suspension, or alternatively directly adsorbed or attached to particles (Kreuter, 2004). This active principle can be a biologically active material or a drug, and encapsulating or attaching such materials onto nanoparticles can make it possible to target organs which were previously inaccessible within the human body (Ehrenberg *et al.*, 2009). Recently, a lot of research has focussed on the use of nanoparticle technologies in drug delivery, specifically to the central nervous system. A review by Kreuter that addresses how drugs are delivered to the brain highlights how the blood-brain barrier has so far proven to be a significant obstacle for drug delivery to tissues within the body (Kreuter, 2013). Several previous studies, investigating the transport of drugs across the blood-brain barrier, found that the use of polymeric nanoparticles enables biological agents such as peptides and macromolecules to access cerebral tissues from the blood stream (Kurakhmaeva *et al.*, 2009; Wohlfart *et al.*, 2012). Questions remain unanswered regarding the mechanism involved in the delivery of the drugs to such previously inaccessible places within the body, leading to recent research into nanoparticle-mediated drug transport, the influence of surface properties and/or targeting ligands (Kreuter, 2013). Consequently nanoscience is becoming increasingly important as an area of research.

1.2 The functionalisation of nanoparticles by a protein corona

Nanomaterials have become increasingly popular in science due to their wide range of applications, both biological (Coppage *et al.*, 2011) and technological (Yang *et al.*, 2012). There has been extensive research into the biomedical uses of nanotechnology due to attractive properties that are enhanced at such a small scale. Nanoscale particles have distinctive

properties; optical, chemical and structural, which set them apart from larger molecules (Yang *et al.*, 2012). One example being the high surface-to-volume ratio, which can enhance catalysis by further exposing the metallic active site (Coppage *et al.*, 2011; Dell'orco *et al.*, 2012). It has been found that interactions between the nanoparticle and their intended biological target, for example biological milieu, depend upon the structure of each individual nanoparticle (Prapainop *et al.*, 2012). This structure is controlled by surface-bound proteins and lipids.

In a biological environment, all nanoparticles may acquire a heterogeneous surface coating of biomolecules, such as protein and lipids, termed a protein corona (Prapainop *et al.*, 2012). There is competition between proteins and other biomolecules to bind to the surface of the nanoparticles (Gebauer *et al.*, 2012). There are many factors which influence how this corona is formed such as size, charge, stability of the nanoparticles and the properties of the proteins themselves (Del Pino *et al.,* 2013). Nanoparticles have high surface free energy, causing molecules, particularly proteins, to adsorb onto their surfaces (Wolfram *et al.*, 2014). Forces including Van der Waals interactions, hydrogen bonds, hydrophobic interactions and pi-stacking interactions are responsible for the adsorption of protein molecules onto the surface of nanoparticles (Saptarshi *et al.*, 2013; Wolfram *et al.*, 2014). Proteins can be adsorbed weakly or strongly onto the nanoparticle surface (Treuel *et al.*, 2014) and form relative soft or hard coronas (Monopoli *et al.*, 2011). Soft protein coronas form on shorter time scales and these then evolve into hard coronas over an incubation period of hours (Monopoli *et al.*, 2011; Gebauer *et al.*, 2012). By contrast, a soft corona involves quick, reversible adsorption of proteins with fast exchange rates (Saptarshi *et al.*, 2013), whereas a hard corona is defined by the adsorption of proteins with relatively slower exchange rates (Monopoli *et al.*, 2011). In bacterial microcompartments (Tanaka *et al.*, 2008), large proteins are often folded into complex structures composed of non-covalent protein-protein interactions (Fletcher *et al.*, 2013). These self-assembled cage-like particles could have useful applications in controlled delivery and release of drugs, sensing and in the preparation of protocells for synthetic biology (Uchida *et al.*, 2007; Agapakis *et al.*, 2012; Hammer *et al.*, 2012).

The protein corona is a major determinant for functionalisation of nanoparticles *in vivo* as it reflects their physical surface properties such as size and shape. Modification of these properties can control the interactive abilities of the nanoparticles and it is often necessary for highly hydrophilic molecules to coat the surface of the nanoparticles to prevent protein adsorption (Yang *et al.*, 2012). This happens as the nanoparticles are coated with molecules specific to the proteins of the associated corona, enabling these molecules to target particular proteins and cause protein misfolding (Prapainop *et al.*, 2012). Such misfolding can initiate access for the nanoparticles into cells which they may not be able to target otherwise via cell-specific uptake. Whilst the protein corona determines the function of the nanoparticles (Yang *et al.*, 2012), the surface of the nanoparticles themselves can also have an effect on the structure of the adsorbed proteins and therefore affect the bio-reactivity of the nanoparticles (Saptarshi *et al.*, 2013). It has been suggested that protein adsorption onto nanoparticle surfaces can be regarded as binding ligands to the nanoparticles (Del Pino *et al.*, 2013). Like other ligands, proteins are able to displace other biomolecules as they adsorb and desorb onto the nanoparticle surface. Proteins are not very stable (Treuel *et al.*, 2014) and so can form certain interactions with different nanoparticle surfaces which could affect the protein conformation (Gebauer *et al.*, 2012). Structural changes may require a strong interaction, but could result in a loss in the biological function of the protein (Treuel *et al.*, 2014). Such changes in protein conformation caused by adsorption of the proteins onto the particle surface could expose new antigenic sites (Lynch *et al.*, 2006) and novel “cryptic” peptide epitopes, as found by Klein and co-workers (Klein *et al.*, 2007). The exposure of such sites could result in an immune response (Brandes *et al.*, 2006), which could ultimately promote autoimmune diseases if launched against a self-protein (Nel *et al.*, 2009).

Being able to reach new areas of biological surroundings with nanoparticles in this way has generated much more research into the use of nanomaterials (Prapainop *et al.*, 2012). It has also highlighted new uses of nanomaterials, for example surface attachment of polysaccharides to nanoparticles can increase the ability of the nanoparticle to permeate cells and therefore improve cancer targeting within the body (Yang *et al.*, 2012).

Dell'orco *et al.* (2012) have investigated the advance in nanotechnology and how it has introduced new devices and procedures. These involve nanoparticles with unique physicochemical properties, which can target and reach parts of the body that have never been accessed before by nanomaterials. The authors of this paper examined computationally whether or not the nanomaterials are always successful in their targeting and delivery and how the protein corona would affect this (Dell'orco *et al.*, 2012).

Nanomaterials and their associated protein coronas stabilise the delivery of drugs *in vitro* (Dell'orco *et al.*, 2012; Dittrich *et al.*, 2012). A study by Dittrich *et al.* has recently suggested that if nanoparticles were coated exclusively in peptides their physicochemical properties could be finely tuned corresponding to their delivery pathway (Dittrich *et al.*, 2012). Interactions between peptides and protein coronas and how these stabilise nanoparticles are of particular interest. Peptides stabilise nanoparticles and allow physical properties such as size and shape to be controlled, it is the interaction between the nanoparticle and the peptide itself that is poorly understood (Coppage *et al.*, 2011).

1.3 Applications of Nanoparticles

Millington *et al.* have investigated how nanoparticles used in sunscreens are able to generate free radicals and reactive oxygen species upon their absorption of ultraviolet rays from the sunlight (Millington *et al.*, 2014). This in-turn can lead to ultraviolet radiation-mediated skin damage (Sander *et al.*, 2002). These nano-sized particles could be modified by the attachment of ligands at the nanoparticle surface to reduce these adverse effects. There are many ways that one can be exposed to nanoparticles, including cosmetics and certain foods, however the main route is inhalation (Ehrenberg *et al.*, 2009). Some nanoparticle activity occurs simultaneously with exposure, even via inhalation, however it has been shown that once inhaled the nanoparticles are able to enter the blood circulation (Nemmar *et al.*, 2002; Ehrenberg *et al.*, 2009). Dell'Orco *et al.* suggest that when nanoparticles are used for drug delivery or imaging, the nanoparticles are required to be injected either intravenously or directly to the target area (Dell'orco *et al.*, 2012).

Often nanoparticles follow different routes within the body before reaching their final target (Ehrenberg *et al.*, 2009), recently research has focused on the interactions of proteins with nanoparticles and whether or not they affect their targeting ability (Almeida *et al.*, 2007; Illum *et al.*, 2007; Tan *et al.*, 2010). Interactions on the surface of nanoparticles have a large effect on where the particle will stop, for example protein adsorption can determine where a particle will target and how it gets there (Ehrenberg *et al.*, 2009). Ehrenberg *et al.* investigated how proteins interacted with polystyrene nanoparticles, and how these particles bound to endothelial cells cultured from human veins. The investigation found that the amount of protein adsorbed onto the nanoparticles was directly related to how they bound to the endothelial cells. They also found that non-specific interactions largely accounted for the interactions between the nanoparticles and the cells (Ehrenberg *et al.*, 2009).

Nanoparticles can have a functional importance for delivering drugs and proteins themselves as they allow proteins and other larger molecules to adsorb onto their surface and pass through barriers and membranes into areas which they are too large to normally access. For example, in the respiratory tract of the human body, the mucosa form a complex barrier which macromolecules such as proteins are unable to filter through (Dombu *et al.*, 2013). Dombu *et al.* have explored different applications of nanoparticles such as cancer therapy, central nervous system targeting and vaccination (Dombu *et al.*, 2012). Adsorbing proteins to nanoparticles can make them more accessible to various parts of the body therefore increasing their therapeutic potential (Dombu *et al.*, 2012). However, once again targeting remains an issue with therapeutic peptides associated to nanoparticles, as this can reduce stability and activity. With vaccination, nanoparticles are able to bind to antigens and deliver them to the required site without degradation (Prieur *et al.*, 1996). Coating the nanoparticles with antigens increase the uptake of the antigens into the cells and can provide immunisation against infections both airborne and blood-borne. Cancer cells over express protein markers, therefore have the potential for protein-protein interactions (Dombu *et al.*, 2013). Protein or peptide based drugs are often developed to target cancer cells as they can take advantage of these protein-protein interactions (Dombu

et al., 2013). Once again, nanoparticles are useful as the proteins themselves are too large to cross many barriers within the body. Specific protein coated nanoparticles have been developed to interact with the protein markers on particular cancerous tumors. Targeting the central nervous system to deliver therapeutic proteins to the brain involves transport through the nasal route. Associating the proteins with nanoparticles increases their bioavailability and targeting power. As with many modern applications of nanoparticles, the exact mechanisms of the protein transport to their target are unknown (Dombu *et al.*, 2013).

The act of coating the nanoparticles with proteins is, as described previously, the formation of a protein corona. Dell'Orco *et al.* state that the protein corona assists with nanoparticles and their therapeutic uses (Hu *et al.*, 2011; Dell'Orco *et al.*, 2012). The protein corona is able to lower the cytotoxicity of the nanoparticles, enabling them to be used in nanomedicine. There have been several investigations into the cytotoxicity of engineered nanoparticles, including silica (Chang *et al.*, 2007), quantum dots (Derfus *et al.*, 2004; Hoshino *et al.*, 2004) and gold nanorods (Hauck *et al.*, 2008), all of which have shown that there is a direct link between the properties of the nanoparticles and their bioavailability. Physicochemical properties of media solutions and the nanoparticles can also be linked. For example, increasing the ionic strength of a solution decreases the electrostatic forces between surfaces which would usually cause them to repel each other. This increases flocculation of nanoparticles, therefore encouraging the nanoparticles to bind to the biological surfaces (Fatisson *et al.*, 2012). Coating the nanoparticle surface with proteins stabilises not only the nanoparticles but also the colloidal suspensions.

1.4 Selenium

Jöns Jacob Berzelius discovered selenium in 1817 (Arner *et al.*, 2012). Even at such an early stage he had noted the similarities between selenium and sulphur, which support the similarities in properties of selenocysteine-containing proteins and those of cysteine containing peptides. Selenate and selenite are two oxidised forms of selenium, selenate being the most oxidised form (Butler, 2012). Selenate is easily reduced and is used as a respiratory

substrate by some bacterial species (Butler, 2012). It has been found that certain bacterial species can act as microbial factories for nanoparticle production, a good example being the bacterium *T. selenatis*, which depends on selenium nanoparticle production to respire selenium-containing oxyanions (Macy *et al.,* 1993).

1.5 *Thauera selenatis*

In 1983 there were environmental problems linked to the agricultural drainage waters in the San Joaquin Valley of California due to a high concentration of selenate, selenite and selenium in these waters (Saiki *et al.*, 1987). These high levels of toxic selenium and it's oxyanions cause problems to aquatic organisms (Saiki *et al.*, 1987), these problems could be aleviated by the reduction of selenate and selenite to elemental selenium (Macy *et al.*, 1989). Elemental selenium is less toxic than selenate (Debieux *et al*., 2011) and is easier to isolate and remove from contaminated water than the highly soluble selenate (Schroder *et al.*, 1997). An organism able to reduce selenate to selenite under anaerobic conditions was isolated from the drainage waters in the San Joaquin Valley of California and incorrectly classified as a *Pseudomonas* species by Macy and co-workers (Macy *et al.,* 1989). A further study carried out by Macy *et al.* classifies *T. selenatis* as a Gram-negative β-proteobacterium able to respire anaerobically using selenium or nitrogen oxyanions as the electron acceptor (Macy *et al.,* 1993). *T. selenatis* is able to simultaneously, and anaerobically, reduce nitrate to nitrous oxide and selenate to selenite. Here, the reduction of selenate to selenite is performed by a dedicated selenate reductase (SerABC), which has been isolated from the bacterium and characterised (Schroder *et al.*, 1997; Krafft *et al.*, 2000). DeMoll-Decker and co-workers reported that selenite reduction to elemental selenium in *T. selenatis* was likely to be catalysed by a periplasmic nitrate reductase (DeMoll-Decker *et al.*, 1993).

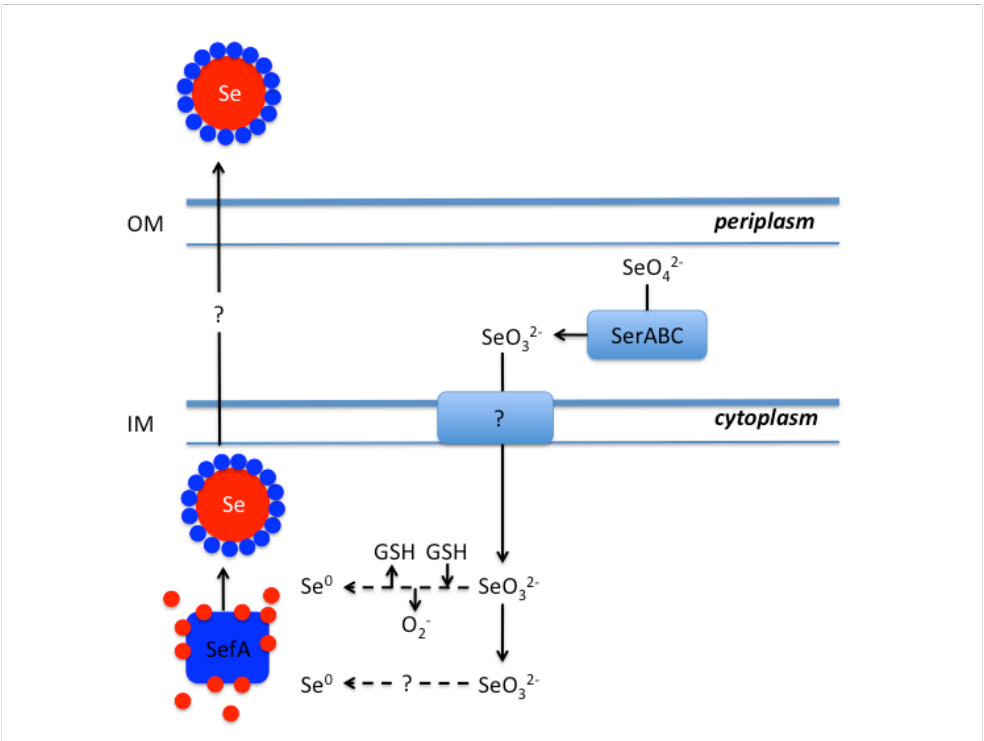

Figure 1.1: A schematic diagram to show the pathway for selenium export within the *T. selenatis* cell.

1.6 Bacterial Selenate Respiration

Macy and co-workers state that *T. selenatis* is able to grow under anaerobic conditions using selenate as the sole electron acceptor. *T. selenatis* can concurrently reduce selenate and nitrate, suggesting that specific reductases act on each (Macy *et al.*, 1993; DeMoll-Decker *et al.*, 1993). The reduction of selenate within *T. selenatis* occurs in the space between the inner and the outer membrane, the periplasmic compartment. The reduction of selenate in the periplasm is catalysed by a trimeric molybdoenzyme, SER, which is the selenate reductase (Schroder *et al.*, 1997). This soluble, trimeric metalloenzyme has both molybdenum- and iron-containing metal centres. It has three subunits; SerA, a catalytic component containing molybdenum and a [4Fe-4S] cluster (Krafft *et al.*, 2000), SerB, an iron-sulphur protein containing one [3Fe-4S] and three [4Fe-4S] clusters (Dridge *et al.*, 2007) and SerC, a haem *b* protein (Lowe *et al.*, 2010). SerD is a cytoplasmic protein which assists with the assembly of SerA (Schroder *et al.*, 1997; Butler *et al.*, 2012). The reduction of selenate requires two electrons from quinol (the Q-pool) (Butler *et al.*, 2012). A study carried out by Lowe *et*

al. found that a di-heme cytochrome of the cyt-c_4 family provides an electron transfer pathway from the Q-pool to SerC (Lowe *et al.*, 2006). The electrons are then transferred through the SerC and SerB to reach the catalytic molybdenum site in SerA, which is where the two-electron reduction of selenate to selenite occurs (Lowe *et al.*, 2006).

Selenite reacts readily with thiols (Painter *et al.*, 1941), and recent research by Debieux *et al.* (2011) suggests that glutathione (GSH), the most commonly reduced thiol in *E. coli*, could assist the bacterial intracellular reduction of selenite. The glutathione reacts with the selenite itself to produce a glutathione reductase, selenodiglutathione (GS-Se-SG). This selenodiglutathione is then further reduced to form an unstable selenopersulfide of the glutathione, $GS\text{-}Se^-$, which then breaks down to form elemental selenium, Se^0, and reduced glutathione (Debieux *et al.*, 2011). *T. selenatis* uses the intracellular reductant, glutathione, to detoxify selenite during the respiration of selenate, leading to a build up of selenium within the cell. It is thought to be necessary for the cell to expel the selenium from within using an export system (Debieux *et al.*, 2011). Ogasawara *et al.* suggest that once selenite has reacted with GSH to produce elemental selenium within Rhodanese, a selenotrisulphide or perselenide intermediate could donate selenium to a protein and in this way provide a selenium delivery system (Ogasawara *et al.*, 2001).

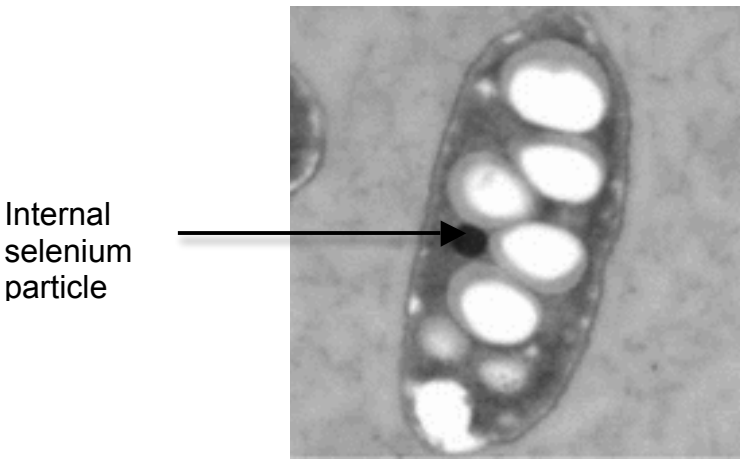

Figure 1.2: Transmission Electron Microscopy (TEM) micrograph of a *T. selenatis* cell taken from the mid-exponential growth phase showing an internal selenium particle (Butler *et al.*, 2012).

Transmission Electron Microscopy (TEM) has shown that as *T. selenatis* cells are grown on selenate, as the growth starts to enter the

stationary phase, elemental selenium particles gather in the cytoplasm (Figure 1.2). Once growth stops, the particles are then observed outside of the cytoplasm, suggesting that they have been excreted from the cell (Butler, 2012). A recent study by Dobias and co-workers, focusing on *E. coli*, shows that in the presence of selenite, there is evidence of selenium interacting with various proteins (Dobias *et al*. 2011). This protein-nanoparticle interaction is said to be a controlling factor throughout the reduction of selenite, in particular where the selenium nanospheres are formed in *T. selenatis* (Butler, 2012).

1.7 SefA

Debieux *et al.* (2011) analysed growth medium of *T. selenatis* following secretion of selenium nanoparticles from the cell cytoplasm during selenate respiration (Debieux *et al.*, 2011; Butler *et al.*, 2012). The protein profile showed a major protein at 94.5 kDa, which is believed to be specific to the reduction of selenite. It is also believed that this protein is related to the export of selenium from the cell and therefore it has been named Selenium Factor A (SefA) (Debieux *et al.*, 2011). SefA has been cloned and expressed in *E. coli* and it has been shown that as selenite is reduced by glutathione, selenium nanoparticles are produced *in vitro* and SefA stabilises the formation of these nanoparticles. The amount of SefA present is directly proportional to the amount of time taken for *T. selenatis* to reduce selenite (Butler *et al.*, 2012). The protein has been characterised and found to be made up of 961 amino acids and have a molecular mass of 95.4 kDa (Debieux *et al*., 2011). SefA is unusual as the five amino acids; alanine, threonine, glycine, valine and aspartate make up 64.3% of the primary sequence (Butler, 2012). There are no cysteine residues in SefA, suggesting that selenium and SefA do not make disulphide bonds, but that they might form weaker interactions via carboxylate ligands. During the characterisation of the protein it was observed that the selenium nanoparticles grow to be up to 130 nm in diameter before they are excreted from the cell (see figure 1.3). Another question surrounding this research is how a particle so large can cross the membrane of the cytoplasm without damaging the cell, and whether or not there are specific factors controlling the size (Butler, 2012).

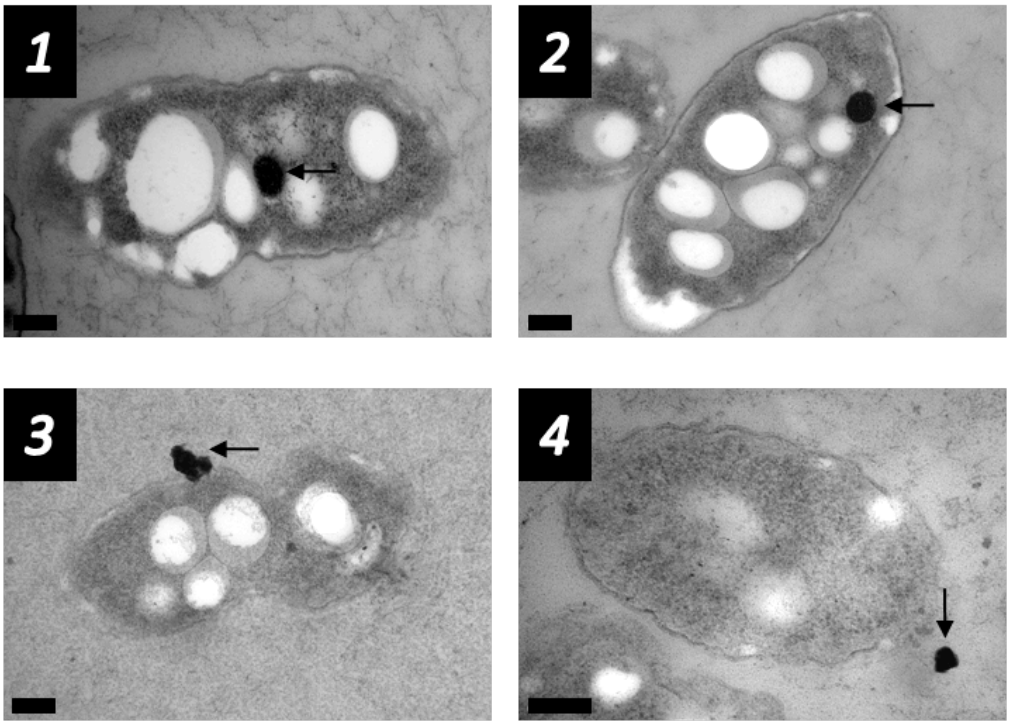

Figure 1.3: Transmission electron micrographs at time points of the growth of *T. selenatis*. 1 and 2 show the appearance of the selenium nanospheres at the late exponential growth phase. 3 and 4 show the stationary growth phases of *T. selenatis*, where the selenium nanospheres appear to have been excreted from the cell. Scale bar represents 200 nm.

Peptides and proteins such as bovine serum albumin (BSA) have been found to stabilise selenium nanoparticles via a non-specific interaction (Bucking *et al.*, 2009). In Bucking's investigation it has been found that the BSA 'caps' the surface of the nanoparticle, suggesting that a similar action could be followed by SefA in *T. selenatis*. If the SefA protein capped the selenium nanoparticles in *T. selenatis*, SefA could provide reaction sites for the assembly of the nanoparticles and in this way prevent particle aggregation (Debieux *et al.*, 2011). It is believed that SefA is exported directly from the cytoplasm, as the protein does not contain an N-terminal signal sequence required for export to the periplasmic compartment of the cell (Debieux *et al.*, 2011). Targeting of the periplasmic compartment via a twin-arginine-translocation (TAT) was also shown to be an unlikely pathway for the protein (Suwa *et al.*, 1997; Debieux *et al.*, 2011). It has been suggested that selenium nanospheres leave the cell via one of two secretion systems. Either the Type 1 Secretion System (T1SS) due to the absence of cysteine residues in SefA (Delepelaire *et al.*, 2004), or the Type 6 Secretion System (T6SS) as all other proteins secreted by this system are similarly not first translocated to the

periplasmic compartment due to the lack of an N-terminal signal sequence (Debieux *et al.*, 2011).

Zhang *et al.* have discovered that a variety of different microorganisms are able to produce extracellular or intracellular selenium nanoparticles via the reduction of selenate and selenite in both aerobic and anaerobic conditions (Narasingarao *et al.*, 2007; Ghosh *et al.*, 2008; Prakash *et al.*, 2009; Zhang *et al.,* 2012). Micro-aerobic conditions were proven to be beneficial to the effects of certain microorganisms on the reduction of selenium oxyanions (Ike *et al.*, 2000; Dungan *et al.*, 2003; Lee *et al.*, 2007). It is easier to characterise extracellular selenium nanoparticles than it is intracellular, as they are easier to isolate from a culture. Oremland *et al.* studied three different selenate respiring bacteria, the investigation focused on whether they produced intracellular or extracellular selenium nanospheres (Oremland *et al.,* 2004). Intracellular selenium deposits have been imaged by electron microscopy in various bacteria, both selenium respiring and selenium resistant, such as *Wollinella succinigenes* and *Chromatium vinosum*. Proposed export methods of extracellular selenium deposits have been cell lysis or a membrane efflux pump (Tomei *et al.*, 1995; Losi *et al.*, 1997). Selenium deposits have been observed accumulating in cytoplasmic compartments of cells, this overload of selenium is rarely tolerated. This calls for the exportation of selenium nanospheres from the cells (Zhang *et al.*, 2012). This export of selenium requires energy, therefore oxygen or another electron acceptor must be present to allow for respiration which releases energy. Zhang and co-workers conducted a study focusing on the reduction of selenite to elemental selenium under oxygen-limited conditions, assisted by yeast cells (Zhang *et al.*, 2012). It has been suggested that these yeast cells transport the over loaded selenium out of the cells under such conditions leading to the formation of extracellular selenium nanoparticles (Zhang *et al.*, 2012). Early studies showed selenium to be present in the cell wall and membrane, the ribosomal fraction and primarily in the cytoplasm. More recently locating the position of elemental selenium within the cell has become more accessible due to electron microscopy.

1.8 The production of selenium nanoparticles

Many nanoparticles have properties which are specific to certain organisms, for example the aquatic bacteria *Leptothrix ochracea* oxidise iron to produce iron oxide nanoparticles (Hashimonto *et al.*, 2007). The biologically-derived iron oxide nanoparticles produced are ocher deposits in irrigation canals, natural streams and ditches (Spring *et al.*, 2006; Emerson *et al.*, 2010). Iron oxide nanoparticles isolated from a water purifying tank in Japan (Hashimonto *et al.*, 2012) have been shown to have applications in carriers for cell culture (Seno *et al.*, 2012) and battery electrodes (Takada *et al.*, 2008). Another example of organism-specific nanoparticles are selenium nanospheres produced in *T. selenatis* during selenate respiration. Selenate is reduced in two steps, via selenite, eventually producing elemental selenium (Debieux *et al.*, 2011). Selenium is an element in group 16 of the periodic table (a chalcogen) which can exist in four oxidation states; -2, 0, +2 and +4 (Butler *et al.*, 2012). It is the two soluble oxyanions, (oxidation states +4 and +6), which are involved in bacterial selenate respiration in *T. selenatis*. The oxidised selenium species with an oxidation state of +4 is selenite (SeO_3^{2-}) and of +6 is selenate (SeO_4^{2-}) (Butler *et al.*, 2012; Butler, 2012). The bacterial respiration process is driven by metalloproteins. Metalloproteins differ from normal proteins in that they bind complex redox-active, metal containing cofactors that can assist electron transfer and therefore catalyse the reductions involved in respiration (Butler, 2012). Selenate, the most oxidised form of non-elemental selenium, is first reduced using two electrons to selenite, which is then reduced further to form elemental selenium (Equation 1 & 2).

$$SeO_4^{2-} + 2H^+ + 2e^- \rightarrow SeO_3^{2-} + H_2O$$

Equation 1: The reduction of selenate to produce selenite (Richardson *et al.*, 2000).

and

$$SeO_3^{2-} + 6H^+ + 4e^- \rightarrow Se^0 + 3H_2O$$

Equation 2: The reduction of selenite to produce elemental selenium (Lloyd *et al.*, 2003).

The elemental selenium (Se^0) produced by *T. selenatis* cells is usually observed as an amorphous red precipitate in batch cultures. However, higher resolution at sub-microscopic scale reveals insoluble, uniform particles that either congregate in the cell or in the surrounding growth medium. Typically there is only one electron dense selenium deposit in each cell, which can be isolated by filtering the growth culture through a fine filter (Butler *et al.*, 2012). It is desirable to obtain these selenium nanospheres in isolation due to the semiconductor and photochemical properties of elemental selenium. These properties lend to their use in solar cells, photocopiers and photographic exposure meters (Johnson *et al.*, 1999).

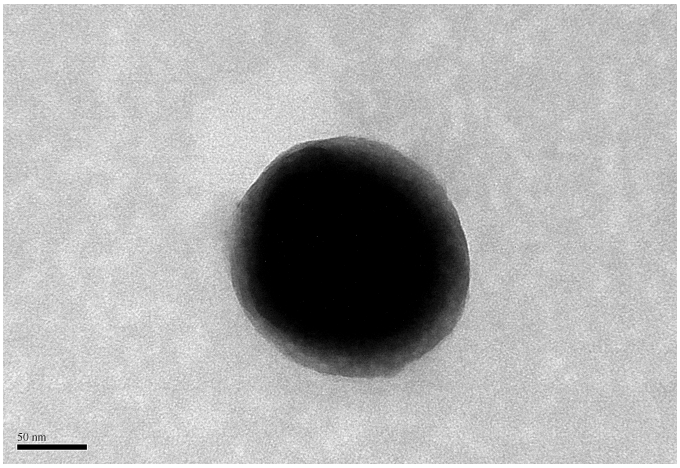

Figure 1.4: TEM micrograph of a secreted selenium nanosphere from a *T. selenatis* cell. Size bar represents 50 nm. (Butler *et al.*, 2012).

Selenium also has important functions within the body such as the formation of selenocysteine and selenoproteins, used to remove products of damage caused by free radicals and reactive oxygen species, therefore bacteria often uptake insoluble selenium within the cell (Heider *et al.*, 1993; Butler *et al.*, 2012). This leads to a build up of toxic selenium within the cytoplasm, a situation that is unsustainable in selenate-respiring organisms (Butler, 2012). A question that surrounds this area of research is how do the bacteria deal with the insoluble selenium nanoparticles. The insoluble selenium deposits in question have been observed in the cytoplasm in the bacterium, as seen in Figure 1.4, suggesting that this is the site of selenite reduction (Butler *et al.*, 2012).

1.9 The abiotic production of selenium nanoparticles

Although there is a lot of evidence of selenium nanospheres being produced biologically via the reduction of selenate and selenite, chemical synthesis is also able to produce selenium particles similar in both size and properties (Oremland *et al.*, 2004). A study involving *E. coli* producing glutathione reductase subsequently found that cells grown in the presence of selenite also produced superoxide dismutase. This suggested that superoxide anions (O_2^-) were also produced and lead Kessi and co-workers to investigate the chemical reduction of selenite by glutathione (Kessi *et al.*, 2004). Ganther proposed the following set of equations to describe the reaction of selenite with glutathione, as selenodiglutathione is a good substrate for glutathione reductase (Ganther *et al.*, 1971).

$$GS\text{-}Se\text{-}SG + NADPH \rightarrow GSH + GS\text{-}Se^- + NADP^+$$

Equation 3: The reaction of selenodiglutathione (Ganther *et al.*, 1971)

$$GS\text{-}Se^- + H^+ \rightarrow GSH + Se^0$$

Equation 4: The reduction of unstable selenopersulphide (Ganther *et al.*, 1971)

Equation 4 shows the formation of elemental selenium and reduced glutathione from the unstable selenopersulphide of glutathione. Kessi *et al.* found that the abiotic reaction that formed the selenodiglutathione was similar to the biological reaction, however much more selenite was reduced in the abiotic reaction (Kessi *et al.*, 2004). In the biological reaction the reduced glutathione is regenerated much like a catalyst however this is not the case in the abiotic reaction. Chemically, there is a build up of oxidised glutathione (GSSG), causing problems for the reaction and therefore slowing down the reaction rate (Kessi *et al.*, 2004). The breakdown of the unstable selenopersulphide of glutathione to elemental selenium and reduced glutathione follows the same process in both the biological and the chemical process.

1.10 Aims and objectives

Research shows that bacteria can play a major part in the reduction of selenium oxyanions to elemental selenium. It is important to understand the role that peptides play in this process and how they interact with the elemental selenium. This project builds on previously published research focussing on proteins secreted during selenium production by the model selenite respiring organism *T. selenatis*. The aims of this present study are:

- To express and purify His-SefA and His-SefA-His.
- To generate selenium nanospheres *in vitro*.
- To analyse the selenium nanospheres in collaboration with NanoSight Ltd via NTA.
- To cleave the N-terminal His-tag from the His-SefA protein to form a non-His-tagged form of the SefA protein.
- To crystalise His-SefA-His in order to resolve the structure of the SefA protein from *T. selenatis*.

2 Materials and Methods

2.1 Expression of His-SefA and His-SefA-His

Previous work (Debieux *et al.*, 2011) isolated a 94.5 kDa protein, SefA, associated with the production of elemental selenium during selenate respiration. Two coding sequences for the SefA protein from *T. selenatis* have been cloned into the pET-33b(+) expression vector. This allowed expression of each recombinant protein from *E. coli* host and subsequent purification from cell-free extracts using affinity chromatography. The first, pET-33b/*His-SefA*, is an expression construct for the SefA protein with a His-tag attached to the N-terminus and the second, pET-33b/*His-SefA-His*, is a construct for SefA expression with a His-tag on both the N-terminus and the C-terminus. Cells (from glycerol stock) containing the relvant expression construct for either His-SefA or His-SefA-His were added to 100 mL Lysogeny Broth (LB) containing kanamycin (50 μg/mL) and chloramphenicol (35 μg/mL). The culture was grown overnight with agitation (250 rpm) at 37°C. 10 mL of this overnight culture was added to 500 mL of fresh LB media and incubated under agitation at 250 rpm at 37°C until the optical density OD_{600nm} was 0.4. At this point the culture was cooled for 30 minutes, Isopropyl β-D-1-thiogalactopyranoside (IPTG) was added to a final concentration of 1 mM before incubating the culture overnight with agitation (250 rpm) at 20°C. The cells were then extracted by centrifugation at 5,000 x *g* at 10°C for 15 minutes, the supernatant discarded, before resuspension in 25 mL of buffer Tris-HCl (pH 7.0), 0.5 M NaCl, 50 mM Imidazole. The cells were stored at -20°C until further use.

Table 2.1: Bacterial strains and plasmids used in this study		
Strains and Plasmids	Characteristics	Reference
E. coli BL21-CodonPlus®(DE3)-RIPL	F–, *dcm*, *omp*T, *hsd*S (rB– mB–), *gal*, λ(DE3)	Stratagene
T. selenatis (ATCC55363)	Selenate respiring, β-subclass of proteobacteria	Macy *et al.*, 1993
pET33b	Kan^r, *lac*I gene, IPTG inducible, P_{T7}	Novagen

2.2 Purification of His-SefA and His-SefA-His

2.2.1 Cell Lysis

Cells were lysed via sonication with a deflection of 10 microns using a programme of 25 seconds on and 35 seconds off, repeated for six cycles. The cell debris were then clarified by centrifugation at 20,000 x *g* at 4°C for 30 minutes The supernatant was retained and either used immediately or frozen at -20°C.

2.2.2 Nickel affinity chromatography

A 20 ml affinity column containing 10 ml ProBond™ Nickel-Chelating Resin was equilibrated with three column volumes of buffer A. The sample was then added to the column and left to bind under gentle agitation for 20 minutes before the resin was left to settle by gravity. The affinity column was washed with two column volumes of buffer A (2.2.3) to remove any unbound sample before one column volume of buffer B (2.2.3) was applied to elute the bound sample. Fractions were collected at the wash steps and elution steps and analysed using SDS-PAGE.

2.2.3 Buffer preparation for purification

Buffer A – 50 mM Tris-HCl, pH 7.0, 0.5 M NaCl, 100 mM imidazole

Buffer B – 50 mM Tris-HCl, pH 7.0, 0.5 M NaCl, 1 M imidazole

Buffer C – 10 mM HEPES, pH 7.0, 0.5 M NaCl

2.2.4 Gel filtration chromatography

A Superdex 200 HiLoad 16/60 (GE Healthcare) 120 ml gel filtration column was equilibrated with one column volume of buffer C (2.2.3) at a flow rate of 1 ml/min. The sample was loaded and eluted over one column volume collecting fractions. Collected fractions were analysed using sodium dodecyl sulphate polyacrylamide gel electrophoresis (SDS-PAGE).

The Superdex 200 gel filtration column was calibrated with the following protein standards: thyroglobulin (669 kDa), apoferritin (443 kDa), β-amylase (200 kDa), bovine serum albumin (66 kDa) and carbonic anhydrase (29 kDa). These protein standards were applied to the Superdex 200 gel filtration column equilibrated in one column volume of 50 mM Tris-HCl, pH 7.5, 100 mM KCl and eluted with this same buffer. The large polymer blue dextran (2000 kDa) was used to determine the void volume (V_o = 39.88 ml). The elution profile (figure 2.1) was used to determine an approximate molecular mass for the proteins using the following equation:

$$Kav = \frac{Ve - V0}{Vt - V0}$$

Equation 5: Calculation of K_{av}. V_e = elution volume of the protein, V_0 = void volume of the column (39.88 ml), V_t = total volume of the column (120 ml).

A rearrangement of the equation of the line of the calibration curve allows the log molecular weight to be calculated:

$$logMW = 0.9028 - Kav0.293$$

Equation 6: Calculation of the log of the molecular weight.

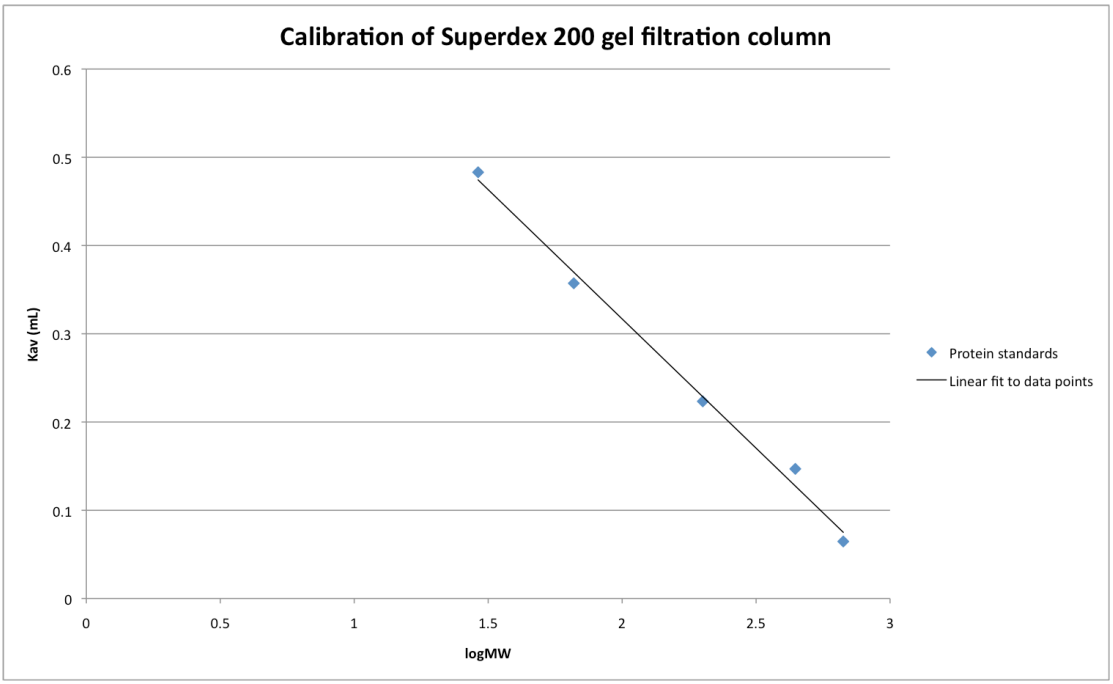

Figure 2.1: The elution profile of protein standards carbonic anhydrase, BSA, amylase, aptoferritin and thyroglobulin (left to right).

2.3 SDS-PAGE

Protein was analysed by SDS-PAGE using pre-cast NuPAGE® Novex® 10% Bis-Tris Gels as per manufacturers instructions.

2.3.1 Stock Solutions

NuPAGE® LDS Sample Buffer (4X):-	40-70% Glycerin 7-13% Sulfuric acid, monododecyl ester, lithium salt
NuPAGE® Reducing Agent (10X):-	500 mM Dithiothreitol
NuPAGE® MOPS SDS Running Buffer (20X):-	50 mM MOPS 50 mM Tris Base 0.1% SDS 1 mM EDTA pH 7.7
NuPAGE® Antioxidant:-	10-30% Dimethylformamide 10-30% Sodium bisulphate

Expedeon Instant Blue Protein Stain:-	0.05% Coomassie Brilliant Blue 2% Ethanol 5% Solubilisers 12% Phosphoric acid

2.3.2 Sample Preparation

5 μl of 4X NuPAGE® LDS Sample Buffer plus 2 μl of 10X NuPAGE® Reducing Agent was added to 13 μl of each sample. The sample buffer and reducing agent denature the proteins and reduce the protein disulphide bonds ready for polyacrylamide gel electrophoresis (PAGE). The mixture was heated at 70°C for 10 min to fully denature the protein before loading it onto the gel.

2.3.3 SDS-PAGE Running

The gel apparatus was set up following the manufacturer's instructions using an XCell SureLock® Mini-Cell. The buffer chamber was filled with 1X NuPAGE® MOPS SDS Running Buffer, with 500 μl of NuPAGE® Antioxidant in the inner chamber. The prepared samples were loaded onto a 10% Bis-Tris NuPAGE® gel along with 5 μl of a molecular weight marker (SeeBlue® Plus2 Pre-Stained Standard). The gel was run at 200 V for 50 min.

2.3.4 Gel Staining Procedure

The SDS-PAGE gel was removed from the gel apparatus and left to stain for 1 hr in Expedeon Instant Blue Protein Stain. The gel was then left to destain in double distilled water (ddH_2O) for 1 hr.

2.4 Western Blot Analysis

Samples were separated on a 10% Bis-Tris SDS gel and the gel was set up in the XCell II™ Blot Module following manufacturer's instructions for the transfer of proteins onto a nitrocellulose membrane ready for immunodetection. The blotting apparatus was cleaned with distilled water (dH_2O) and methanol and then set up with three layers of 3 mm blotting paper, one layer of filter paper, the SDS gel, one layer of nitrocellulose

membrane, one layer of filter paper and a further three layers of 3 mm blotting paper. All blotting paper, filter paper and transfer membrane was pre-soaked in 1 x transfer buffer (25 mM Tris-HCl pH 7.5, 200 mM glycine). The proteins were transferred to the nitrocellulose membrane at 30 V for 60 min. The nitrocellulose membrane was then soaked in 10-20% dried milk diluted in 1 x wash buffer for 30-60 min with agitation.

5 x Wash Buffer

1M Tris-HCl pH 5.6	50 ml/L
NaCl	146 g/L
Tween 20	2.5 ml/L

The nitrocellulose membrane was then washed 3 x 5 min in 1 x wash buffer before incubation overnight at 4°C with the primary antibody Monoclonal Anti-polyHistidine antibody produced in mouse (4 μl diluted in 20 ml of 1 x wash buffer). The membrane was then washed twice quickly, once for 15 min, then twice for 5 min in larger volumes of 1 x wash buffer. The nitrocellulose membrane was then incubated at room temperature with agitation for 1 hr with the secondary antibody Anti-Mouse IgG Alkaline Phosphatase (AP) Conjugate (4 μl diluted in 20 ml of 1 x wash buffer). The membrane was then washed again twice quickly, once for 15 min, then twice for 5 min in larger volumes of 1 x wash buffer. The nitrocellulose membrane was then drained of wash buffer and incubated at room temperature with agitation in 10 ml of Western Blue stabilized substrate for Alkaline Phosphate for 5 min. After 5 min bands should begin to develop on the nitrocellulose membrane.

2.5 Crystallisation of His-SefA-His

2.5.1 Preparation of protein for crystallisation

After gel filtration chromatography, the fractions containing purified protein were concentrated to ~ 10 mg/ml as in methods 2.4.

2.5.2 Initial crystal trials

Microbatch crystallisation trials were set up in a Hampton Research 96 well plate using an Oryx 6 crystallization robot (Douglas Instruments, UK). A JCSG screen was used (Molecular Dimensions Laboratories). The final droplet volume was varied between 1 μl and 2 μl depending on how much protein solution was available. The droplet contained a 50:50 ratio of protein to screen and each droplet was then covered with Al's oil (50:50 mix of silicon oil to paraffin). The plates were stored at 18 °C and regularly checked for crystal growth using a light microscope.

2.5.3 Preparing crystals for data collection

Crystals were frozen using a cryo-protectant (10 mM HEPES Na salt, pH 7.5, 0.1 M CAPS, 1 M NaBr, 40 % MPD). The crystals were removed from the droplet and placed in the cryo-protectant before being frozen directly in liquid nitrogen and taken to the Diamond Light Source (Oxford, UK). This is the UK's national synchrotron facility where data is collected under cryo cooled conditions.

2.6 Protein concentration determination

Proteins were concentrated using a Millipore Amicon Ultra centrifugal spin concentrator at 5000 x *g* and 4°C.

2.6.1 Bio-Rad protein assay

The Bio-Rad protein assay was carried out using a microplate reader following the standard procedure for microtiter plates. The dye reagent was prepared by diluting 1 part Dye Reagent Concentrate to 4 parts dd. H_2O. This was filtered through a Minisart® Plus syringe filter (0.2 μm) and kept at room temperature. Five dilutions of a protein standard, Bovine Serum Albumin (BSA), were prepared: 0.05 mg/ml, 0.1 mg/ml, 0.2 mg/ml, 0.3 mg/ml and 0.5 mg/ml. The protein solutions were assayed in triplicate. 10 μl of each standard and sample solution was pipetted into separate microtiter plate wells. 200 μl of diluted dye reagent was added to each well. The sample and reagents were mixed well using a microplate mixer. The microtiter plates were

incubated at room temperature for at least 5 min but for no longer than 1 hr Absorbance was measured at 595 nm.

2.6.2 NanoDrop

Protein concentration was determined using a NanoDrop 2000c UV-Vis Spectrophotometer (A_{280}). This technology requires blanking with the protein buffer then using 2 μl of sample to detect protein concentration.

2.7 *In vitro* formation of selenium nanospheres

Selenium nanoparticle formation assays were performed in 50 mM Tris-HCl buffer (pH 8), supplemented with protein, 5 mM reduced glutathione and 0.75 mM selenite at room temperature in quartz cuvettes. The reaction was carried out under anaerobic conditions so all solutions were sparged with nitrogen including the cuvette itself prior to reduction with reduced glutathione. The formation of selenium nanospheres was measured spectrometrically at 400 nm over a period of 400 s. The selenium nanoparticle formation assays were repeated at a range of protein concentrations (0.5 μg/ml – 50 μg/ml).

2.8 Nanoparticle analysis in collaboration with NanoSight Ltd

2.8.1 Nanoparticle Tracking Analysis (NTA)

NTA tracks the Brownian motion of nanoparticles in liquid suspension on a particle-by-particle basis. The Stokes-Einstein equation (equation 7) relates Brownian motion to particle size.

$$Dt = \frac{TK_B}{3\pi\eta d}$$

Equation 7: Stokes-Einstein equation where Dt = particle diffusion coefficient, T = temperature (Kelvin), K_B = Boltzmann's Constant, η = solvent viscosity and d = the sphere-equivalent hydrodynamic diameter.

The NTA was carried out using a NanoSight LM10-HS instrument, which uses a laser light to illuminate the nanoparticles within a 0.3 ml sample introduced to the viewing unit. Results were displayed as a frequency size distribution graph and output to spreadsheet. Still video clips showing nanoparticles were also obtained.

2.8.2 Zeta Potential

Zeta potential was measured using a ZetaSight system which allowed the zeta potential of nanoparticles in aqueous suspension to be measured on a particle-by-particle basis. An electric field was applied to the nanoparticles, which caused them to move and the NanoSight technique recorded the apparent drift velocity of each particle.

2.9 Protein modification

Both recombinant proteins, His-SefA and His-SefA-His were modified by cleaving the N-terminal His-tag off of the protein to form both SefA and SefA-His. This was carried out using a Thrombin CleanCleave™ Kit from Sigma-Aldrich.

2.9.1 Sample Preparation

All protein to be modified must be previously purified by nickel affinity chromatography and then exchanged into 50 mM Tris-HCl, pH 8.0, with 10 mM $CaCl_2$.

2.9.2 Washing Resin

The thrombin-agarose resin (thrombin-agarose 50 % suspension in 50 % glycerol, 20 mM Tris-HCl, pH 8.2) was thoroughly resuspended to make a homogeneous slurry. A 100 µl aliquot was removed and gently spun in a microcentrifuge at 500 x *g* (2,500 rpm) for 10 min to pellet the resin. The supernatant was poured off carefully. 500 µl of 1 X cleavage buffer (50 mM Tris-HCl, pH 8.0, 10 mM $CaCl_2$) was added to gently resuspend the pellet by inverting the tube. This was then centrifuged at 500 x *g* for 10 min and the supernatant was poured off carefully. This washing step was repeated.

2.9.3 Cleavage Reaction

100 µl of 10 X cleavage buffer (500 mM Tris-HCl, pH 8.0, 100 mM $CaCl_2$) was added to the centrifuged beads to gently resuspend them. 1 mg of protein was added and the final volume was brought to 1 ml with water. The cleavage reaction was incubated with gentle agitation at room temperature for

24 hr. Aliquots were removed at 1, 2, 4, 6 and 24 hours and gently centrifuged to remove the resin and analyze the supernatant for cleavage by SDS-PAGE and Western Blotting.

2.9.4 Recovery of the fusion protein

The cleavage reaction was transferred to the column, once the resin had settled the eluent was drained and collected. The resin was rinsed with 5 bed volumes of 1 x cleavage buffer and the eluent collected. All eluents were combined.

2.9.5 Separating the protein from the cleaved His-tag

The His-tags need to be separated from the protein that has undergone the cleavage reaction.

The separation of His from SefA was carried out collecting the sample flow through from a nickel affinity column. A 10 ml nickel affinity column was washed with 4 x 10 ml buffer A (2.2.3). The protein sample was added and agitated for 20 min. The column was left to settle before the protein was collected and the protein concentration was determined via NanoDrop (2.7.2). The column was washed with 2 x 10 ml buffer B to remove the His-tags.

3 Probing protein-mediated assembly of selenium nanospheres by recombinant SefA

3.1 Introduction

It has been found that in the selenate respiring bacterium *T. selenatis*, solid selenium deposits are produced during selenate respiration (Macy *et al*., 1989). This precipitated selenium is red and the deposits are spheres with a diameter of approximately 130 nm (Butler *et al.*, 2012). Analysis of the growth medium over time has shown that these selenium nanospheres are exported out of the cell during the exponential growth phase and it is thought that a selenium export factor protein facilitates this exportation. This protein has been calculated to have a mass of 94.5 kDa and has been previously cloned and expressed in *E. coli* and the recombinant His-tagged protein purified (Debieux *et al.*, 2011).

Two recombinant His-tagged forms of SefA have been previously expressed and purified in *E. coli*, the aim of this work is to see what role the recombinant, non-His-tagged SefA protein (rSefA) plays in selenium nanosphere assembly. It is possible that the rSefA protein will behave more similarly to the protein isolated from the growth medium of *T. selenatis*. Sequence inspection of the translated open reading frame for SefA, within the pET-33b/*His-SefA* vector, reveals that the N-terminal His-tag of His-SefA may be cleaved using a Thrombin proteolytic site.

Upon the cleavage of the N-terminal His-tag a new form of the SefA protein will be produced with no His-tags. The non-tagged protein and the cleaved His-tags will be separated via nickel affinity chromatography before investigating the effect of this native protein on selenium nanosphere assembly. Selenium nanoparticles can be produced *in vitro* to form similar particles to those produced in the selenate respiring bacterium *T. selenatis*. In this study a variety of different concentrations of rSefA will be used to investigate what effect the protein has on the assembly and properties of these nanospheres.

3.1.1 Specific aims and objectives

- Express and purify the recombinant His-SefA protein.
- Cleave the N-terminus His-tag from the His-SefA protein to produce the non-His-tagged SefA form, rSefA.
- Investigate the effect of rSefA protein on selenium nanosphere formation via NTA.

3.2 The preparation of rSefA from His-SefA

To obtain a 'His-tag free' form of the SefA protein (rSefA), the N-terminus His-tag had to be cleaved from the His-SefA form of the protein. Looking at the pET-33b(+) vector it can be seen that the N-terminus His-tag could be cleaved at the Thrombin site and carried out using a Sigma Aldrich Thrombin CleanCleave™ Kit.

Cells harbouring a recombinant form to express the His-SefA protein were over-expressed in *E. coli* BL21 CodonPlus (DE3)-RIPL cells. A culture containing the cells expressing the His-SefA protein, kanamycin and chloramphenicol in LB broth was grown overnight at 37°C with agitation. Fresh LB media was inoculated with this overnight culture and incubated under agitation at 37°C until the optical density (OD_{600nm}) was 0.4. Once this optical density had been reached, the culture was cooled for 30 mins prior to the addition of IPTG. The culture was then incubated once more under agitation at 20°C. The cells were then extracted by centrifugation and resuspended before the cells were lysed by sonication and clarified. The His-SefA protein was then purified using nickel affinity chromatography, where the purified protein was eluted in 50 mM Tris-HCl, pH 7.0, 0.5 M NaCl, 1 M imidazole (figure 3.1).

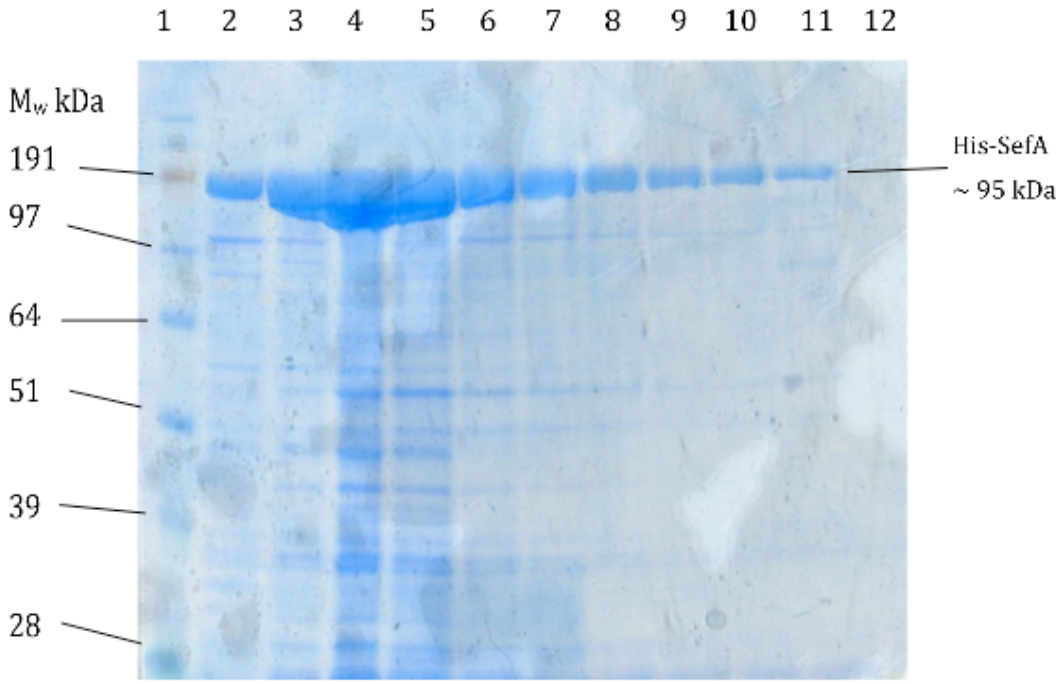

Figure 3.1: SDS-PAGE analysis of His-SefA purified by nickel affinity chromatography. Lane 1 = Pre-Stained protein standard. Lanes 2-11 show elutions from nickel affinity chromatography.

This purified protein was added to the thrombin-agarose resin, following the procedure for the Thrombin CleanCleave™ Kit (materials and methods 2.10) and the reaction was incubated for 24 hours at room temperature with gentle agitation. 100 μl aliquots were taken at time points of 1, 2, 4, 6 and 24 hours and analysed by SDS-PAGE to monitor the progress of the cleavage reaction (figure 3.2). A major protein band was seen on the developed SDS-PAGE gel at approximately 95 kDa, consistent with the expected size and thus the presence of SefA. As the rSefA protein has no His-tags attached to either the N-terminus or the C-terminus, Western Blot analysis (materials and methods 2.5) was used to confirm the cleavage of the N-terminal His-tag from His-SefA. The removal of the N-terminal His-tag can be seen in figure 3.3.

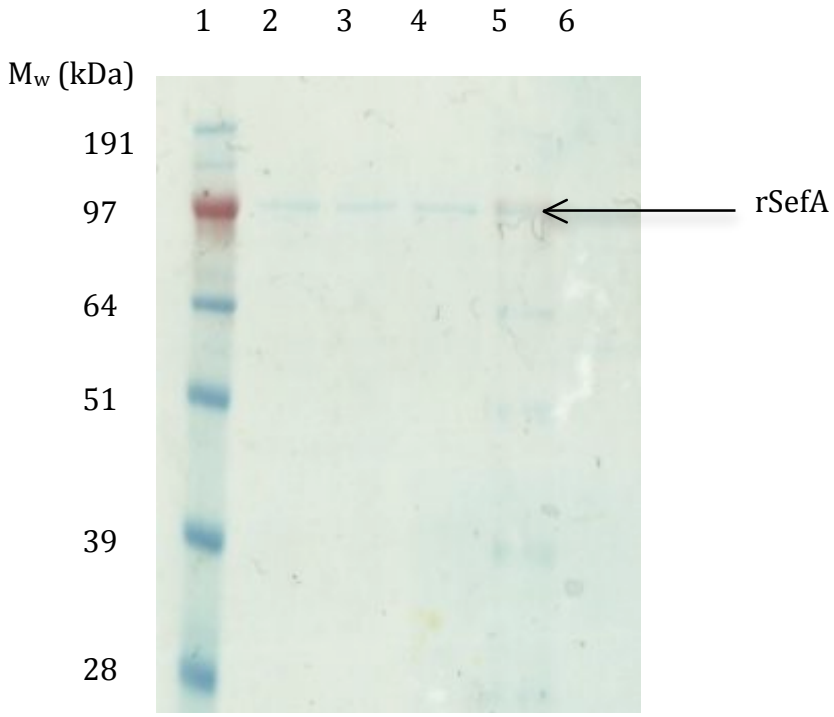

Figure 3.2: SDS-PAGE analysis of the cleavage of the N-terminal His-tag from His-SefA (1 mg/ml). Lane 1 shows Pre-Stained protein standard, lane 2 shows the cleavage reaction at t=1 hr, lane 3 shows t=4 hr, lane 3 shows t=6 hr, lane 4 shows t=24 hr and lane 5 shows rSefA.

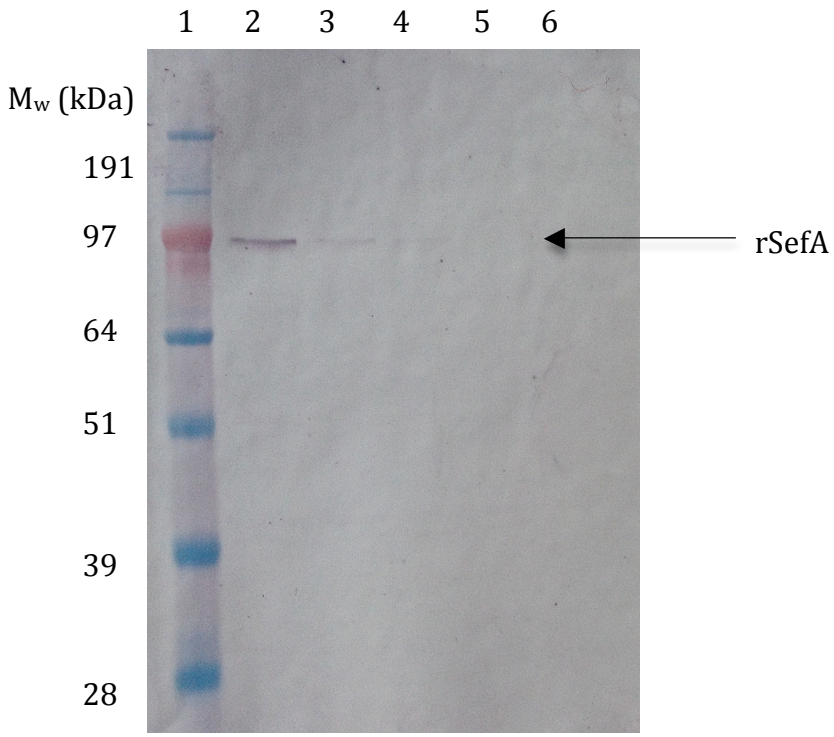

Figure 3.3: Western Blot analysis of the cleavage of the N-terminal His-tag from His-SefA. Lane 1 shows Pre-Stained protein standard, lane 2 shows the cleavage reaction at t=1 hr, lane 3 shows t=4 hr, lane 3 shows t=6 hr, lane 4 shows t=24 hr and lane 5 shows rSefA.

3.3 *In vitro* formation of selenium nanospheres stabilised by rSefA

Preliminary studies showed that Se^0 produced *in vitro* had a wide range of sizes, unlike the selenium deposits produced in *T. selenatis* (Debieux *et al.*, 2011). The red selenium deposits were formed during the anaerobic reaction between reduced GSH (5 mM) and selenite (0.75 mM). It was necessary for the molar ratios of GSH:selenite to be > 4:1 to ensure that the GS-Se-SG was reduced to GSSeH to be reduced further to Se^0 (Debieux *et al.*, 2011). The formation of selenium nanospheres was measured spectrometrically at 400nm in the presence of the rSefA protein (0.5 μg/ml, 1 μg/ml, 5 μg/ml, 10 μg/ml and 50 μg/ml). The reaction was performed in triplicate at each different protein concentration and the formation of these selenium nanoparticles as a function of time can be seen in figure 3.4. A plot of final absorbance plotted against protein concentration can be seen in figure 3.5.

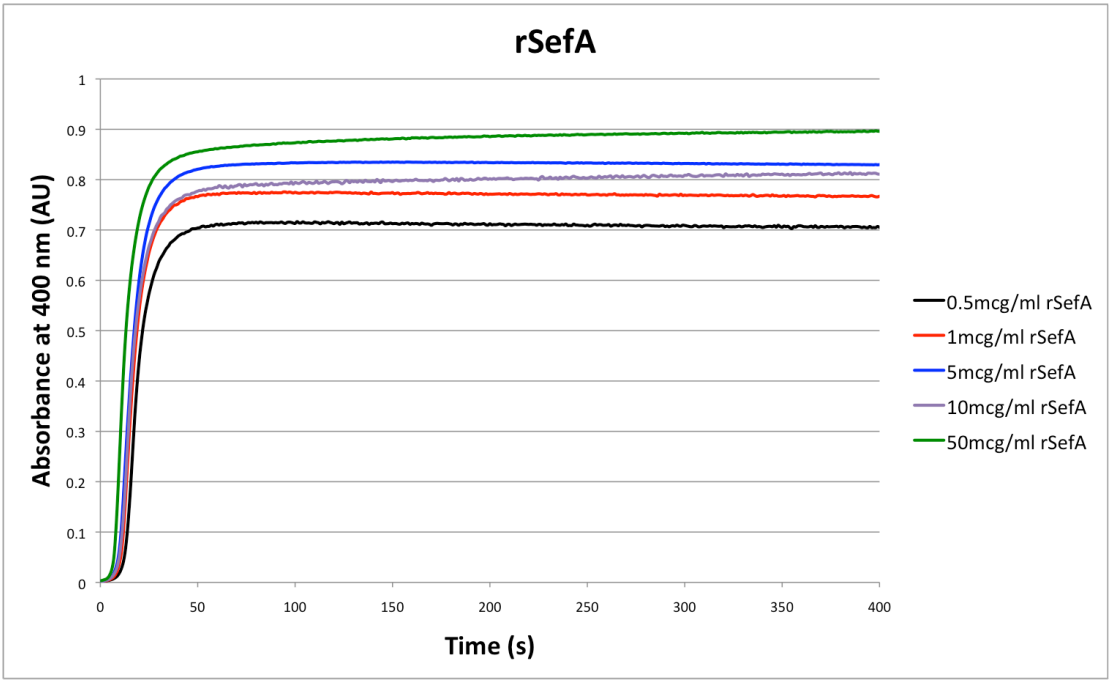

Figure 3.4: The formation of selenium nanospheres measured spectrometrically at 400 nm. This is an average representation of all three runs at different protein concentrations.

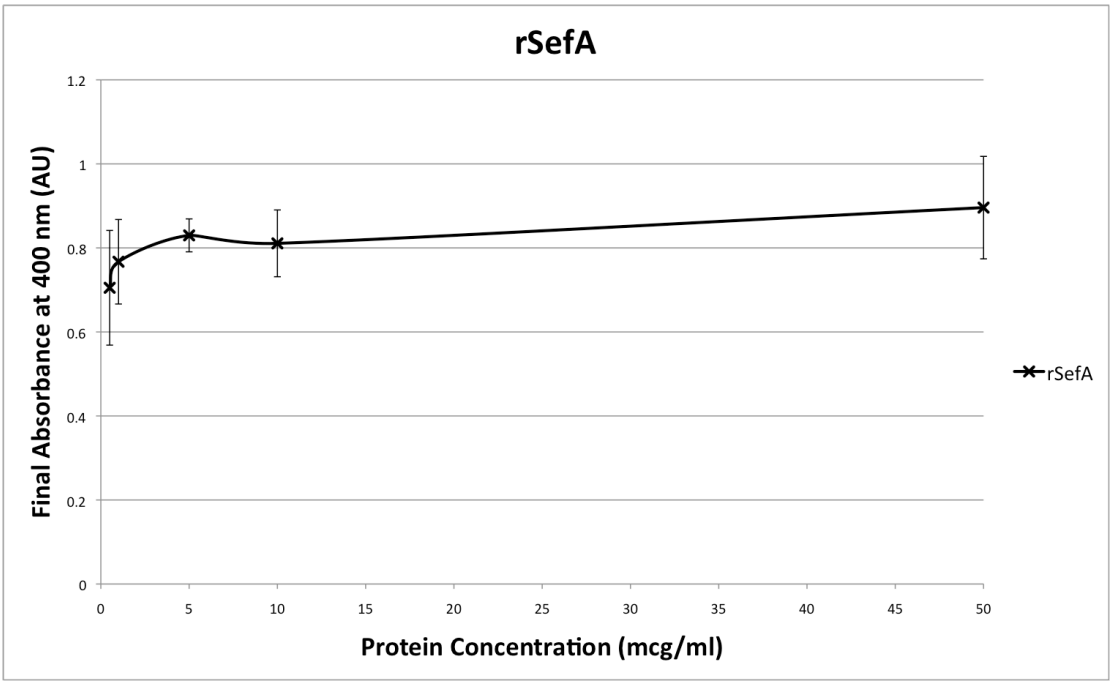

Figure 3.5: A plot of final absorption against protein concentration. This is an average representation as the reaction was run in triplicate at each protein concentration.

Figure 3.4 shows an increase in absorbance with time as the concentration of rSefA increases. The initial formation of particles (0-5 s) shows a slightly slow rate of formation before this rate increases at approximately 5 s. The higher the concentration of the protein the quicker the higher rate of formation is initiated. Figure 3.5 shows a general trend of an increase in final absorption as the protein concentration increases.

3.4 Nanoparticle tracking analysis of selenium nanospheres stabilised by rSefA

Nanoparticle tracking analysis of the selenium nanospheres tracks the Brownian motion of each nanoparticle individually and, with application to the Stokes-Einstein equation, allows particle size to be determined. Nanoparticle tracking analysis was applied to each sample of selenium nanospheres produced as described in 3.3. Nanoparticle tracking analysis produces a video of the nanoparticles in suspension, a time frame of the selenium nanoparticles stabilised by 5 μg/ml rSefA can be seen in figure 3.6.

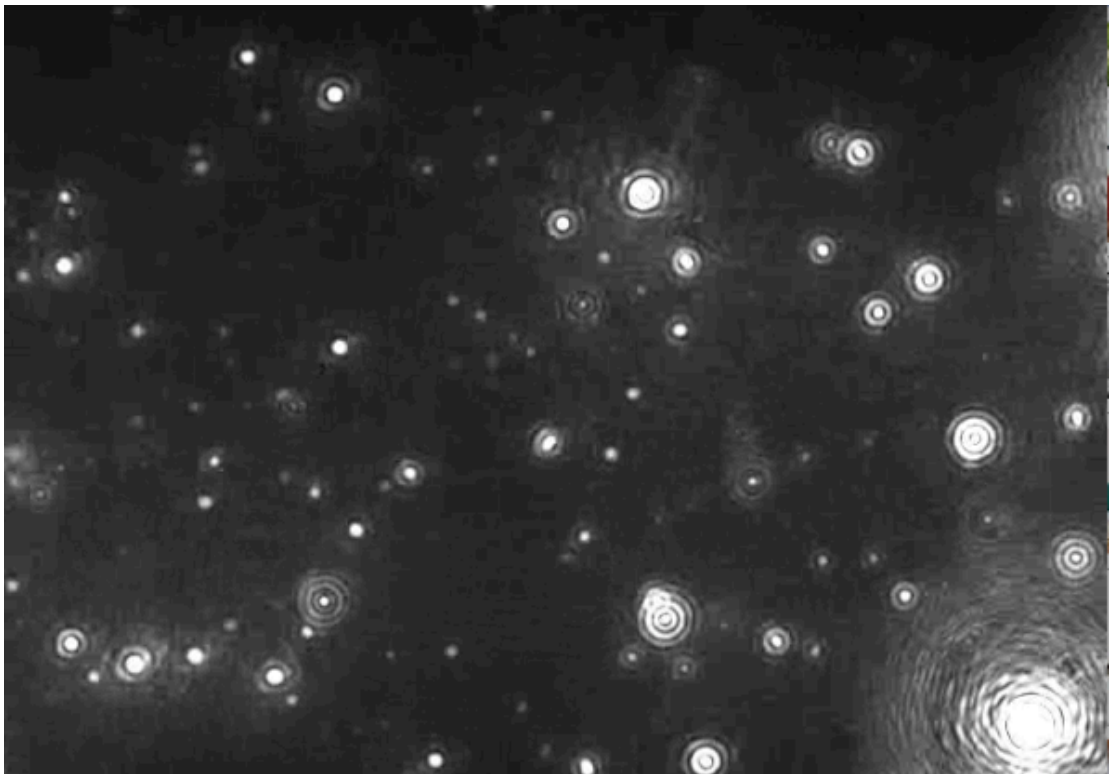

Figure 3.6: A still image of selenium nanoparticles stabilised by 5 μg/ml rSefA. The dots represent selenium nanospheres produced *in-vitro* in the presence of 5 μg/ml rSefA moving due to Brownian Motion.

Plots of concentration against particle size in triplicate of selenium nanosphere samples can be seen in figures 3.7, 3.8 and 3.9 and a plot of mean particle size against protein concentration in figure 3.10. Three separate reactions were analysed individually.

Figures 3.7-3.9 show that in general, at low concentrations of rSefA there is a narrow size distribution of selenium nanoparticles (25-150 nm). However, at higher concentrations of the protein the size distribution is a lot broader (25-250 nm). Figure 3.8 shows a slight variation as it is in fact 5 μg/ml of rSefA, which produces selenium nanospheres with the most narrow size distribution. Figure 3.10, showing mean particle size against protein concentration, shows that as protein concentration increases, the mean particle size also increases. The 'error bars' shown in the figure do not represent error, but the size distribution of the particles formed at each protein concentration. Again here you can see that the size distribution is increasing in range as the protein concentration increases.

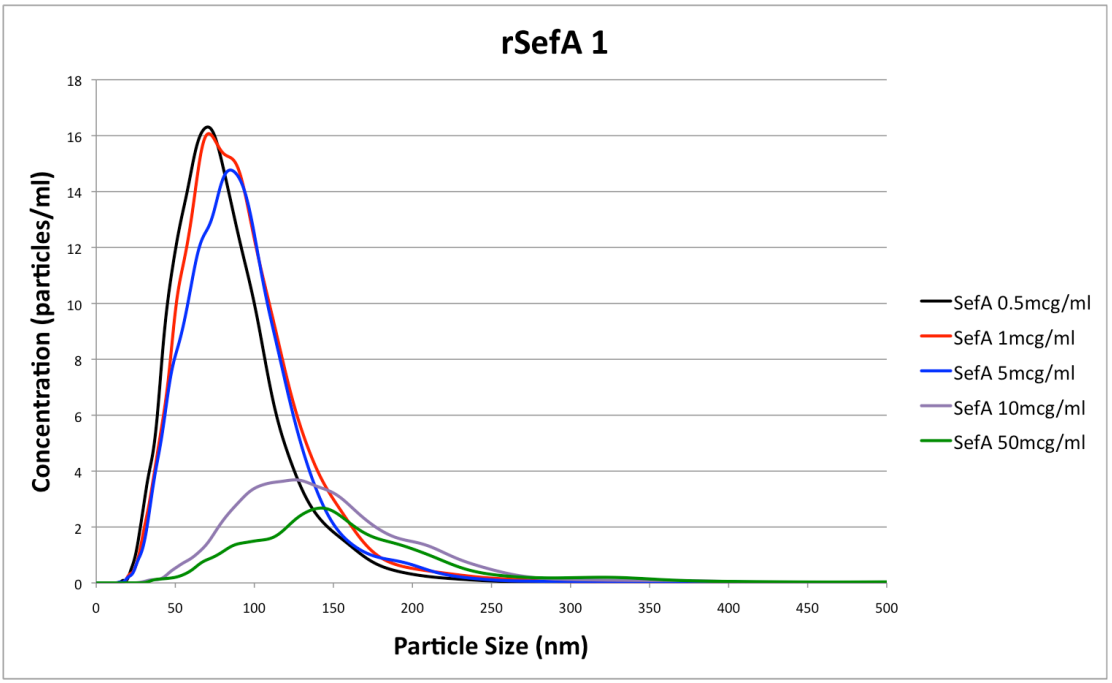

Figure 3.7: Particle size against particle concentration from NTA for reaction 1 over a range of protein concentrations.

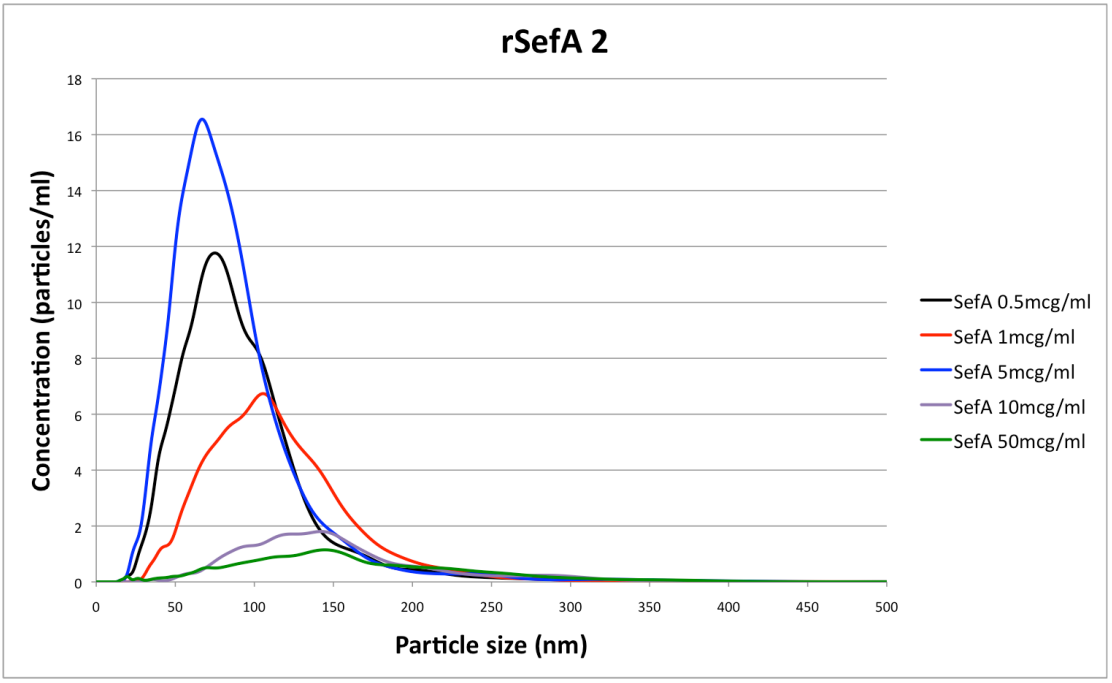

Figure 3.8: Particle size against particle concentration from NTA for reaction 2 over a range of protein concentrations.

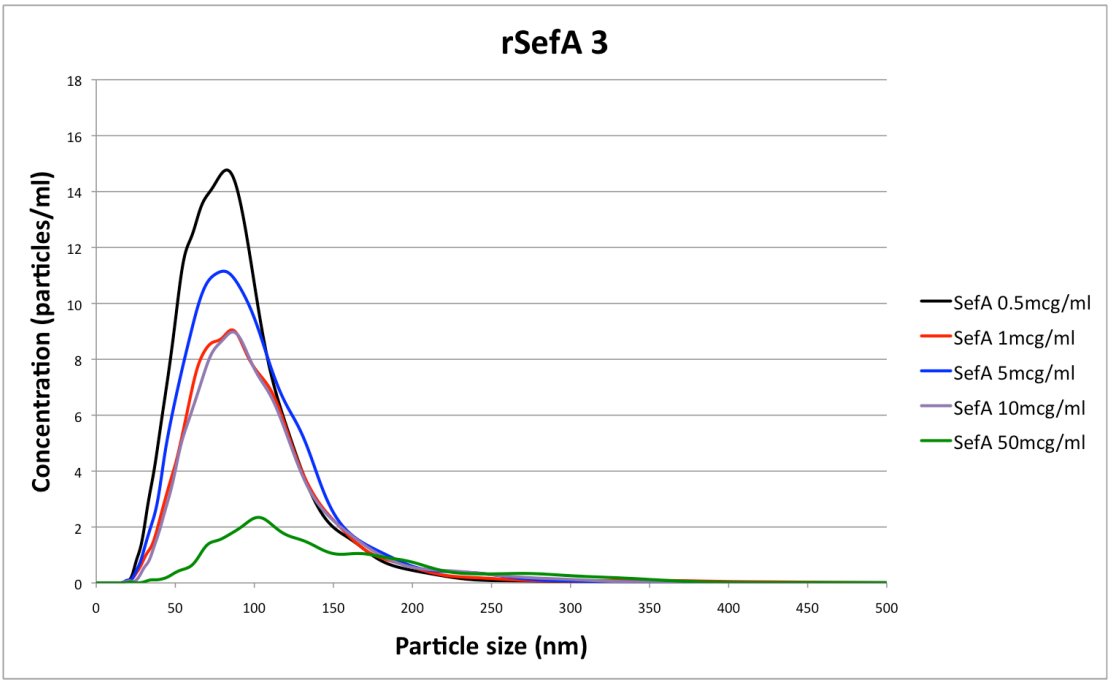

Figure 3.9: Particle size against particle concentration from NTA for reaction 3 over a range of protein concentrations.

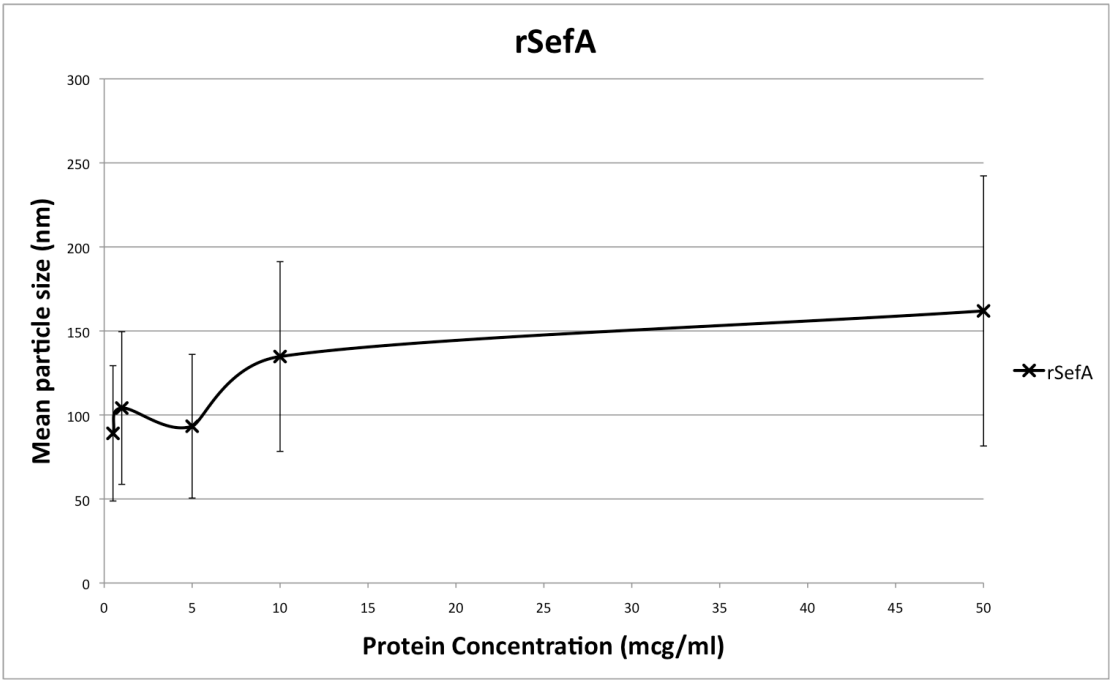

Figure 3.10: An average representation of mean particle size against protein concentration for selenium nanospheres produced in the presence of rSefA.

3.5 Discussion

Preliminary studies (Debieux *et al.*, 2011) showed that His-SefA was not capable of forming selenium nanospheres with a controlled narrow size distribution *in vitro* as seen in *T. selenatis*. This study forming selenium deposits in the presence of the rSefA protein focuses on investigating whether there is a trend in the size and size distribution of the nanospheres produced. The rSefA protein was formed by the cleavage of the N-terminal His-tag of His-SefA at the Thrombin site. This form of the protein, containing neither an N-terminal or C-terminal His-tag, was added to the reaction between reduced GSH and selenite to determine the effect of it's presence on the resulting selenium nanospheres. The reaction was monitored spectrometrically and a general trend can be seen of an increase in absorbance with time as the concentration of rSefA increases. This increase in absorbance suggests that more red selenium nanospheres have been formed and so an increase of protein concentration sees an increase in the amount of selenium formed. As the concentration of rSefA present increased, the particles formed during the reaction had intensified in colour. The plot of final absorbance against protein concentration further confirms this as it shows an increase in final absorbance as protein concentration increases.

The data sets collected from NTA allowed particle size against concentration of the particle size to be plotted and therefore enabled the distribution in size of the particles to be seen. The nanospheres formed at the lowest concentration of rSefA (0.5 μg/ml) showed a narrow size distribution, with a high concentration of particles between 50-100 nm. As the protein concentration increased, the size distribution of the nanoparticles broadened, with selenium nanospheres produced in the presence of 50 μg/ml rSefA showing a lower concentration of particles over a larger scale of 25-250 nm. A trend can be seen of increasing particle size with increasing protein concentration, as well as an increase in final absorbance and an increase in particle size. This suggests that at higher protein concentration not only is more selenium produced but these selenium nanospheres are also larger than those produced at lower protein concentrations. Debieux and co-workers found that selenium nanospheres secreted by *T. selenatis* during selenate

respiration were approximately 130 nm in diameter (Debieux *et al.*, 2011). By contrast, these selenium nanospheres produced *in vivo* in the presence of the recombinant SefA protein produce selenium nanospheres ranging from a mean particle size of ~85 nm, at the lowest protein concentration (0.5 μg/ml), and ~167 nm at the highest protein concentration (50 μg/ml). It has been shown that nanoparticles produced *in vitro* in the presence of 10 μg/ml rSefA are approximately 130 nm in size. This could suggest that *T. selenatis* has an internal SefA concentration of 10 μg/ml to produce stable nanoparticles of this size.

Bucking and co-workers have investigated how nanoparticles are stabilised by protein interactions (Bucking *et al.*, 2009). They have suggested that BSA acts as a stabilising ligand which coats quantum dots. If SefA 'coated' the selenium nanoparticles in this way perhaps it too would have a stabilising effect on these elemental selenium deposits. SefA could be coating the selenium nanospheres and self-assembling it's protein corona into a nano-cage (Fletcher *et al.*, 2013). Fatisson *et al.* discovered that surface charge has an effect on the bioavailability of nanoparticles (Fatisson *et al.*, 2011). The addition or removal of a His-tag from the SefA protein could be affecting the overall surface charge of the SefA-selenium nano-cage. Although I don't believe that the removal of the His-tag would have an effect on the SefA protein, I do think that it could have an effect on the nanocage itself.

SefA homologues have been found in two strains of *Nitrosomonas* and figure 3.11 shows the sequence alignment of SefA with these two strains (AL212 and Is79A3). Strain AL212 has been used for ammonium sulphate reduction (Suwa *et al.*, 1997) and other strains have been shown to produce intra- and extracellular particles. The overall identity between the protein and the two *Nitrosomonas* strains is low however between the first 25 N-terminal residues there is 60% identity (Butler *et al.*, 2012). Suwa and co-workers have shown electron micrographs showing extracellular particles which could be acting in a similar way to the selenium deposits produced in *T. selenatis* (Suwa *et al.*, 1997).

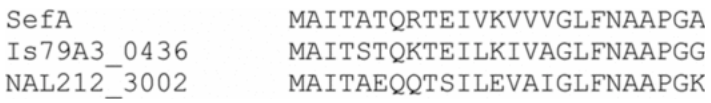

Figure 3.11: Sequence alignment of SefA, Is79A3 and AL212 (adapted from Butler *et al.*, 2012)

This suggests that the N-terminus of SefA could be important in the assembly of the protein and could have a key role in the protein-protein interactions, or indeed the protein-nanoparticle interactions. Del Pino and co-workers discuss how protein adsorption onto nanoparticles resembles ligand binding (Del Pino *et al.*, 2013). This could suggest that the N- and C-terminal His-tags are acting as ligands attached to the SefA protein. If so, this could affect the way in which particles assemble when the N-terminus and C-terminus of SefA are blocked in His-SefA and His-SefA-His. The removal of this N-terminal His-tag and the exposure of the N-terminus of SefA could be important in selenium nanoparticle assembly.

4 Investigating the impact of differentially tagged SefA variants on assembly of selenium nanospheres

4.1 Introduction

Having explored the assembly of selenium nanospheres in the presence of the rSefA protein, the effect of His-tagging the protein on these nanoparticles was investigated. Two His-tagged forms of SefA had been previously expressed (Debieux *et al.,* 2011) one with a His-tag only on the N-terminus (His-SefA) and one with a His-tag on both the N-terminus and the C-terminus (His-SefA-His). Both of these forms of SefA were expressed in LB Broth and purified by nickel affinity chromatography and gel filtration chromatography. These His-tagged forms of SefA were added to the reaction between reduced GSH and selenite and the reaction was measured spectrometrically, at 400 nm, to monitor the formation of selenium deposits. This involved measuring absorbance as a function of time, carrying out nanoparticle tracking analysis with an industrial collaborator and, in one particular case, measuring the zeta potential.

Previous work by Debieux *et al*. has shown that selenium nanospheres produced *in vitro* in the presence of His-SefA form nanospheres of 300 nm in diameter (Debieux *et al*., 2011). These particles are much larger than both those formed in *T. selenatis* during selenate respiration and those formed *in vitro* in the presence of the rSefA protein. This chapter will be looking to see if there are any similarities in the size of the nanospheres as protein concentration is increased across the different forms of the SefA protein. As the presence of the form of SefA with a His-tag on the N-terminus produces larger nanospheres than the rSefA protein, it may be expected that the form with a His-tag on both the N-terminus and the C-terminus may produce even larger selenium nanoparticles. By investigating how the addition of His-tags onto SefA affects the properties of these selenium nanospheres, it may be possible to begin to hypothesise how the protein interacts with the nanoparticles within *T. selenatis* and actually exports them out of the cell.

4.1.1 Specific aims and objectives

- Express and purify the recombinant His-SefA and His-SefA-His proteins.
- Investigate the effect of His-tagging the SefA protein on selenium nanosphere formation via NTA.
- Investigate how colloidally stable the selenium nanospheres are by determining zeta potential.
- Attempt to crystallise the His-SefA-His protein in order that its structure could be determined.

4.2 The expression and purification of His-SefA and His-SefA-His

The two protein constructs were over-expressed in *E. coli* BL21 CodonPlus (DE3)-RIPL cells. An overnight culture was grown at 37°C with agitation containing the glycerol stock for the appropriate bacterial strain, antibiotics and LB broth. This culture was then used to inoculate fresh LB broth and was then incubated under agitation at 37°C until the optical density (OD_{600nm}) was 0.4. Once the optical density had reached 0.4 the culture was cooled for 30 minutes before IPTG was added. Further incubation of the culture under agitation took place at 20°C. The cells were then extracted by centrifugation and resuspended before the cells were broken open by sonication and clarified by further centrifugation. Both proteins were then purified using nickel affinity chromatography, where the purified protein was eluted in 50 mM Tris-HCl, pH 7.0, 0.5 M NaCl, 1 M imidazole. A further purification step was necessary so both proteins were also purified by gel filtration chromatography where the pure protein was eluted in 50 mM Tris-HCl, pH 7.5, 100 mM KCl. SDS-PAGE analysis of the proteins purified by both nickel affinity chromatography and gel filtration chromatography can be seen in figures 3.1, 4.1 and 4.2. The main protein band in both images is shown at approximately 95 kDa, which confirms the presence of the SefA protein.

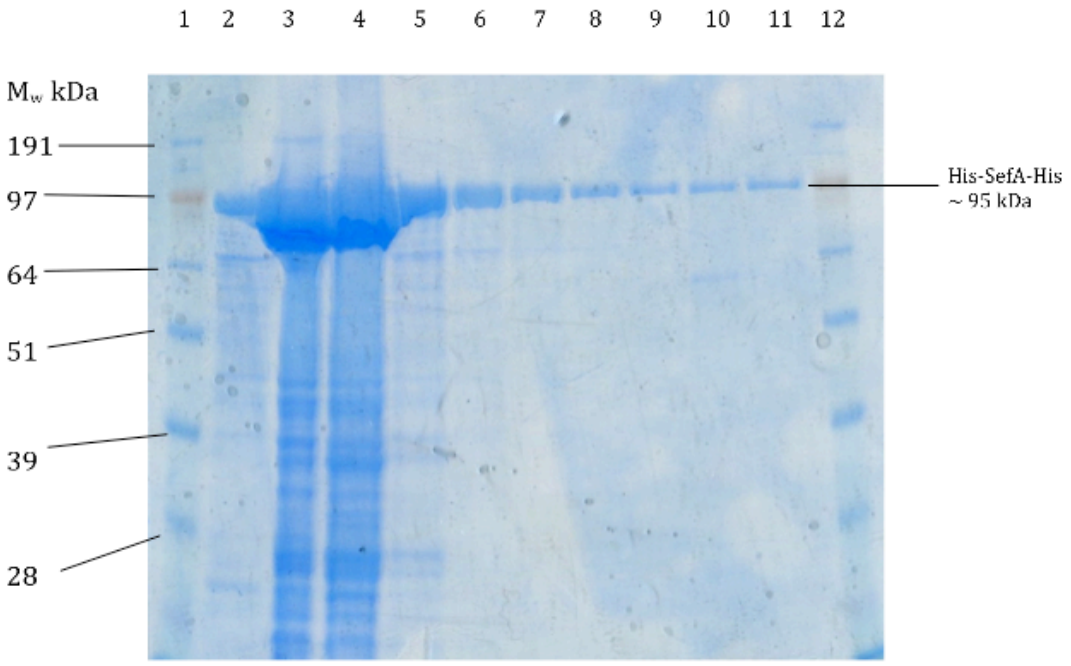

Figure 4.1: SDS-PAGE analysis of His-SefA-His purified by nickel affinity chromatography. Lane 1 = Pre-Stained protein standard. Lanes 2-11 show elutions from nickel affinity chromatography.

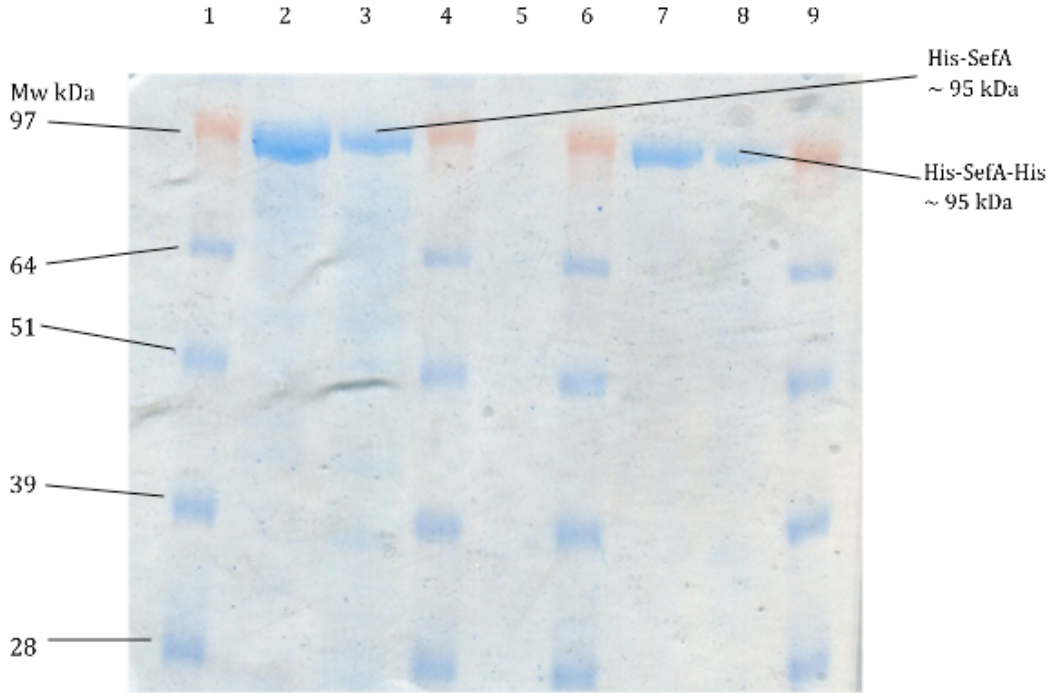

Figure 4.2: SDS-PAGE analysis of His-SefA and His-SefA-His purified by gel filtration chromatography. Lanes 1,4,6 and 9= Pre-Stained protein standard, Lanes 2 and 3 show His-SefA after gel filtration and lanes 7 and 8 show His-SefA-His after gel filtration.

4.3 *In vitro* formation of selenium nanospheres in the presence of His-tagged SefA

The reaction between reduced glutathione and selenite in the presence of His-tagged SefA was investigated. Primarily the reaction was undertaken in the presence of His-SefA, the form of SefA with a His-tag on the N-terminus, and secondly in the presence of His-SefA-His, the form with a His-tag on both the N-terminus and the C-terminus of the protein. The reaction was repeated with both proteins at the same range of protein concentrations as with the native SefA (0.5 μg/ml, 1 μg/ml, 5 μg/ml, 10 μg/ml and 50 μg/ml) and each reaction was undertaken in triplicate. The formation of the red selenium nanoparticles was measured spectrometrically at 400 nm, a plot of absorbance as a function of time across the different protein concentrations can be seen in figure 4.3 in the presence of His-SefA and in figure 4.4 in the presence of His-SefA-His.

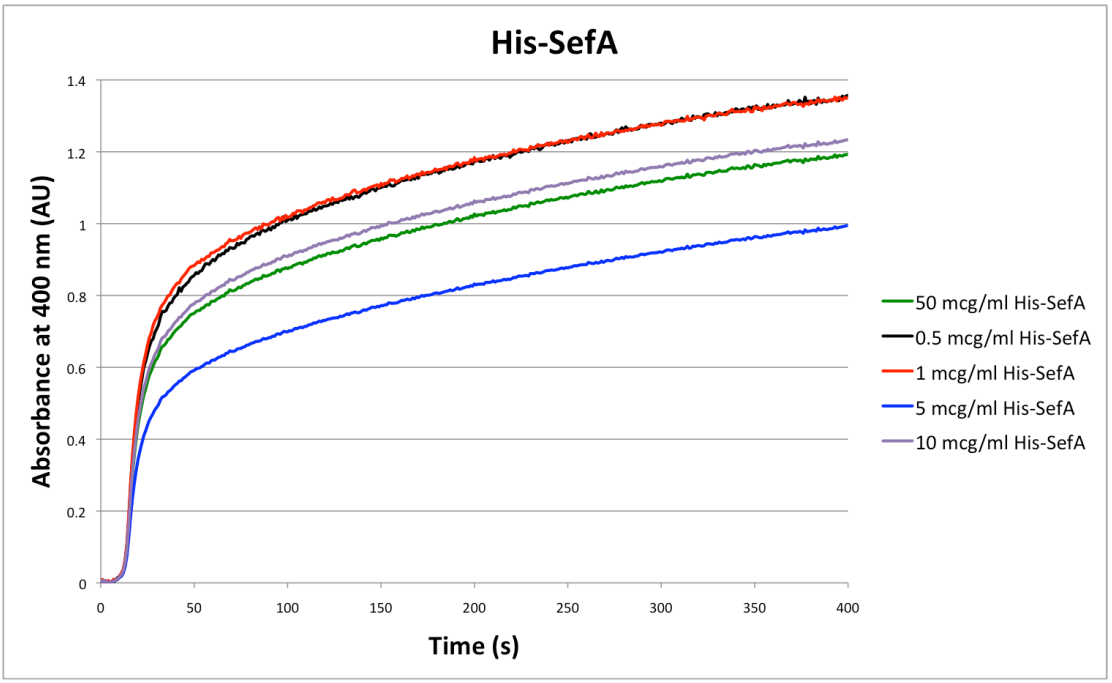

Figure 4.3: The formation of selenium nanospheres produced in the presence of His-SefA was measured spectrometrically shown in this plot of time against absorbance.

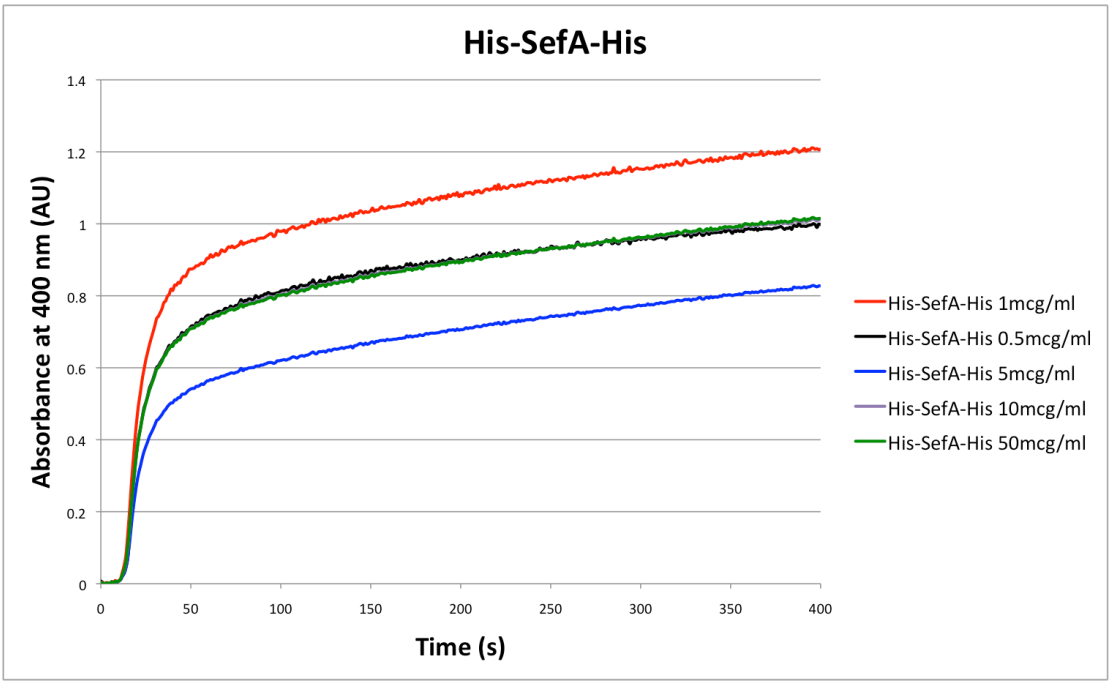

Figure 4.4: The formation of selenium nanospheres produced in the presence of His-SefA-His was measured spectrometrically shown in the plot of absorbance against time.

Figure 4.3 shows a general decrease in absorbance as the concentration of His-SefA increases, whereas the formation of selenium nanospheres produced in the presence of His-SefA-His (figure 4.4) shows an increase in absorbance with increasing protein concentration. Plots of final absorbance against protein concentration can also be seen in figures 4.5 and 4.6. These further confirm the trends outlined above. An increase in the concentration of His-SefA shows a decrease in final absorbance of the selenium nanospheres, whereas an increase in the concentration of His-SefA-His shows an increase in final absorption. The colour intensity of the nanoparticles formed in the presence of these His-tagged proteins can be seen in figures 4.7 and 4.8. In the presence of both His-SefA and His-SefA-His the colour intensity of the nanospheres is decreasing with an increase in protein concentration.

Figure 4.5: A plot of final absorbance for the nanospheres produced in the presence of His-SefA at different protein concentrations. This is an average representation.

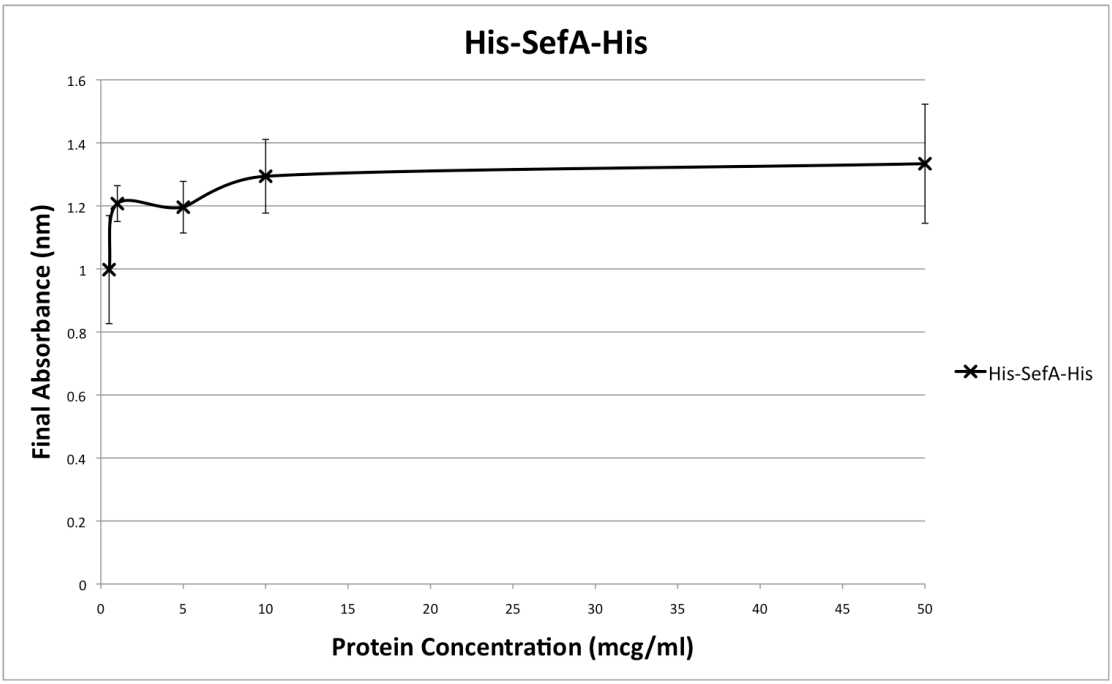

Figure 4.6: An average representation of final absorbance against protein concentration for those particles produced in the presence of His-SefA-His.

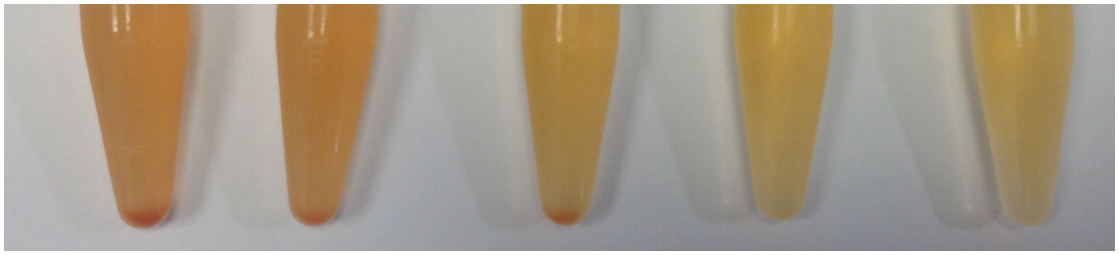

Figure 4.7: The selenium nanospheres formed in the presence of 0.5 μg/ml, 1 μg/ml, 5μg/ml, 10 μg/ml and 50 μg/ml (from left to right) His-SefA.

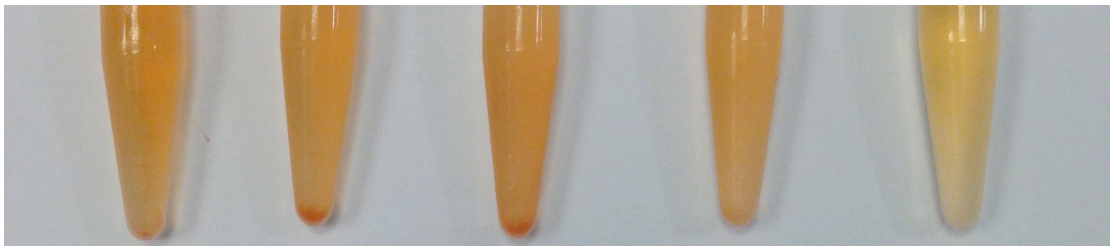

Figure 4.8: The selenium nanospheres formed in the presence of 0.5 μg/ml, 1 μg/ml, 5μg/ml, 10 μg/ml and 50 μg/ml (from left to right) His-SefA-His.

4.4 Nanoparticle Tracking Analysis to investigate the effect of His-tagging the Selenium Export Factor on the assembly of selenium nanospheres

Particle size of the selenium nanoparticles formed in the presence of both His-SefA and His-SefA-His was determined via NTA in collaboration with NanoSight Ltd. NTA tracks the Brownian motion of the nanospheres on a particle-by-particle basis and particle size can be determined using the Stokes-Einstein equation. A video of the nanoparticles in suspension is produced during the analysis and a still of the nanospheres in the presence of 5 μg/ml of His-SefA can be seen in figure 4.9 and those in the presence of 5 μg/ml of His-SefA-His can be seen in figure 4.10.

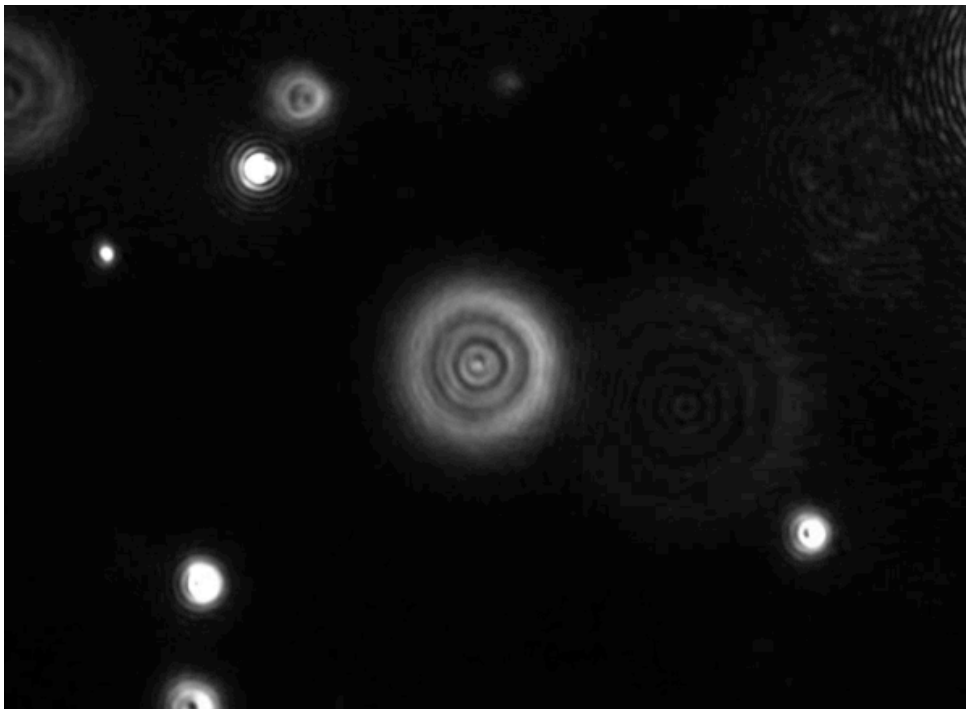

Figure 4.9: A still image of selenium nanoparticles stabilised by 5 μg/ml His-SefA. The dots represent selenium nanospheres produced *in-vitro* in the presence of 5 μg/ml His-SefA, moving due to Brownian motion.

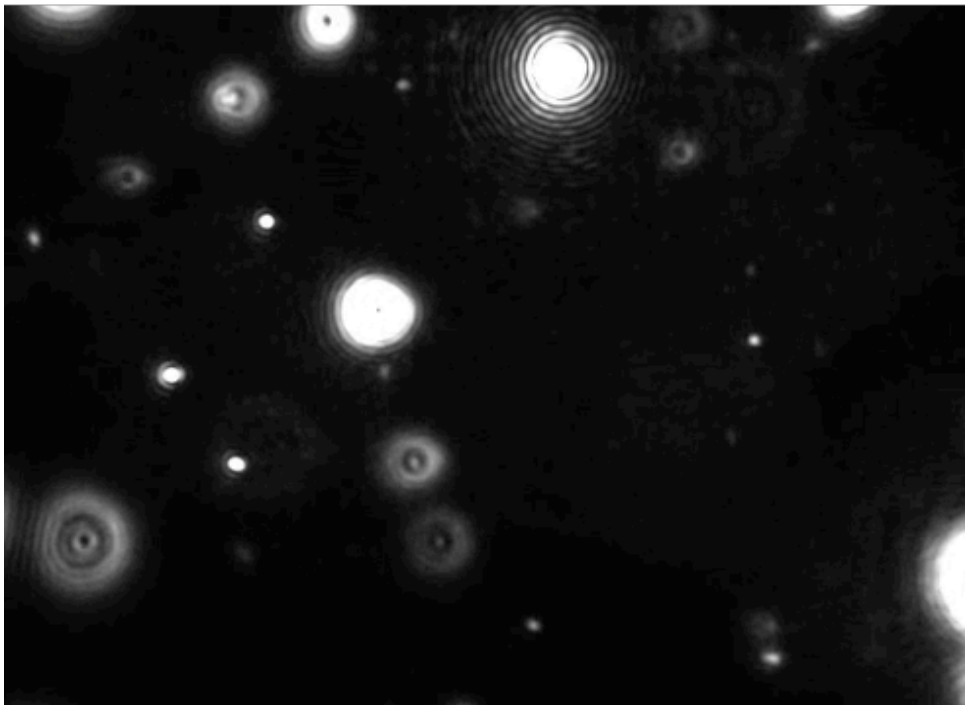

Figure 4.10: A still image of selenium nanoparticles stabilised by 5 μg/ml His-SefA-His. The dots represent selenium nanospheres produced *in-vitro* in the presence of 5 μg/ml His-SefA-His, moving due to Brownian motion.

Figures 4.11-4.13 and 4.14-4.16 show the size distributions of the nanospheres produced at different concentrations of His-SefA and His-SefA-His.

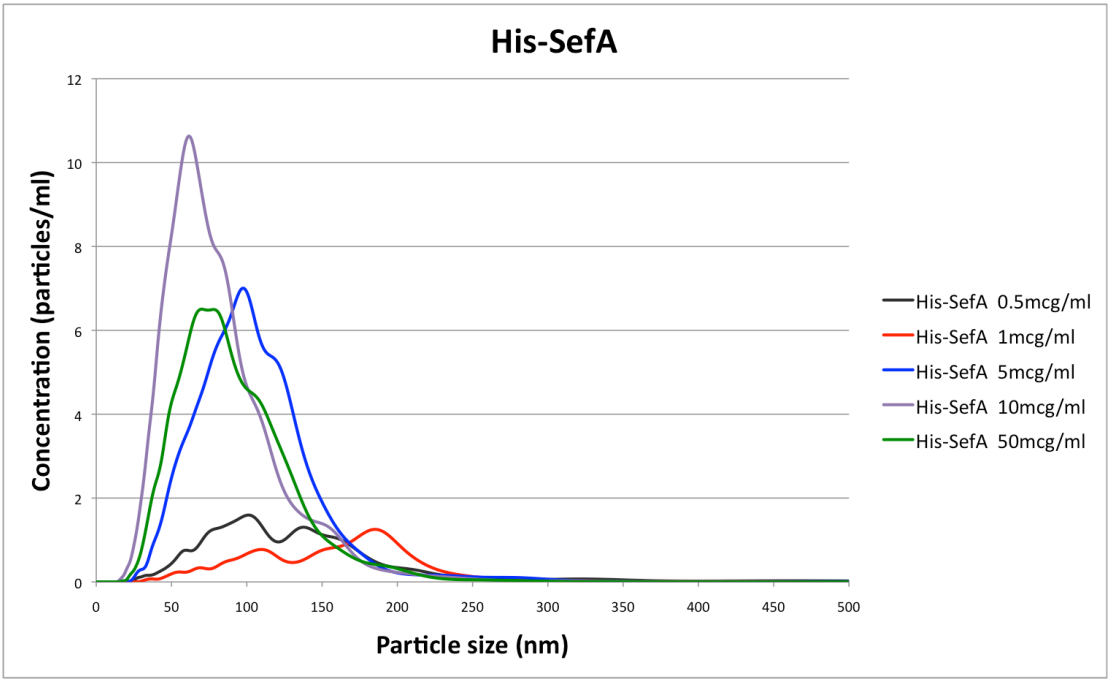

Figure 4.11: Particle size distribution of selenium nanospheres produced in the presence of His-SefA in reaction 1.

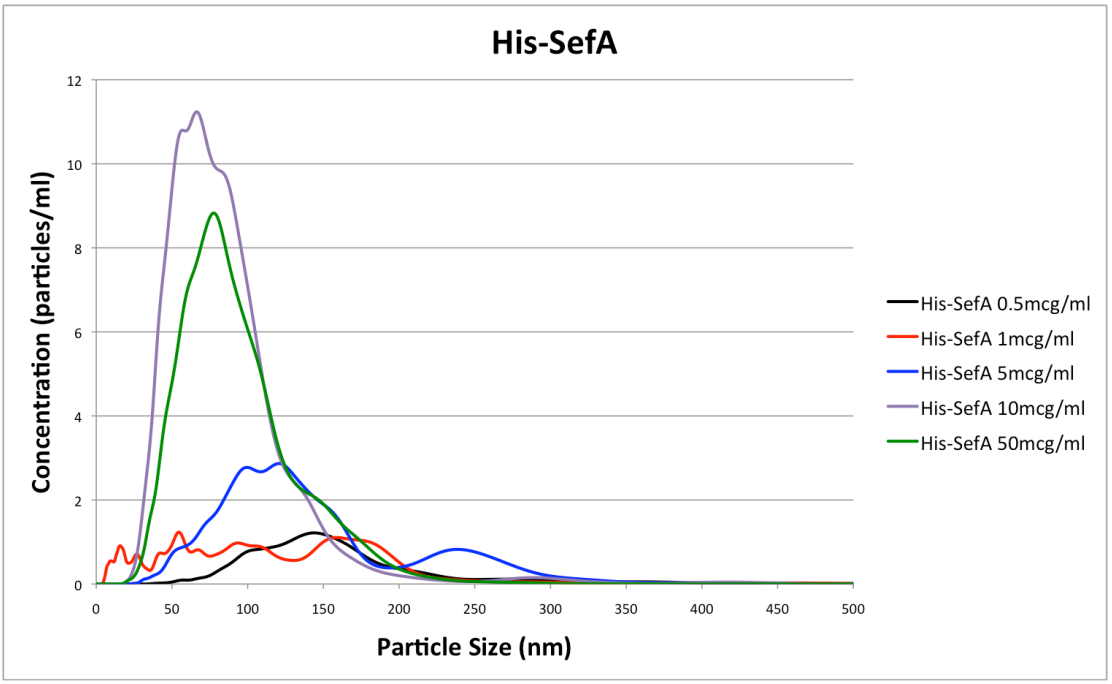

Figure 4.12: Particle size distribution of selenium nanospheres produced in the presence of His-SefA in reaction 2.

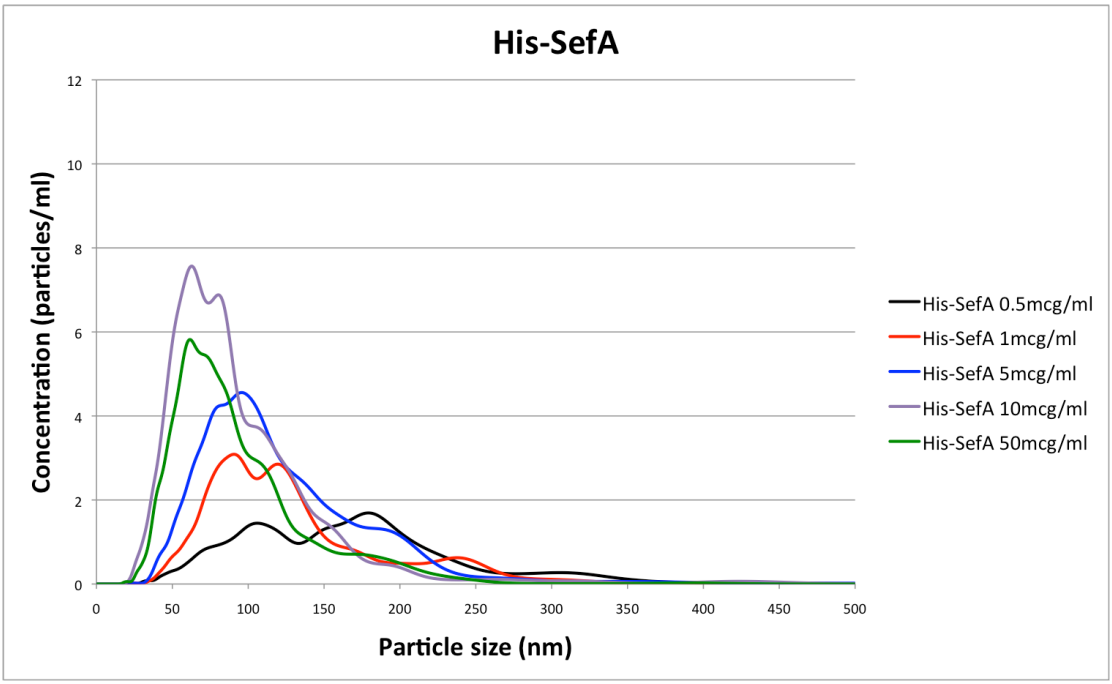

Figure 4.13: Particle size distribution of selenium nanospheres produced in the presence of His-SefA in reaction 3.

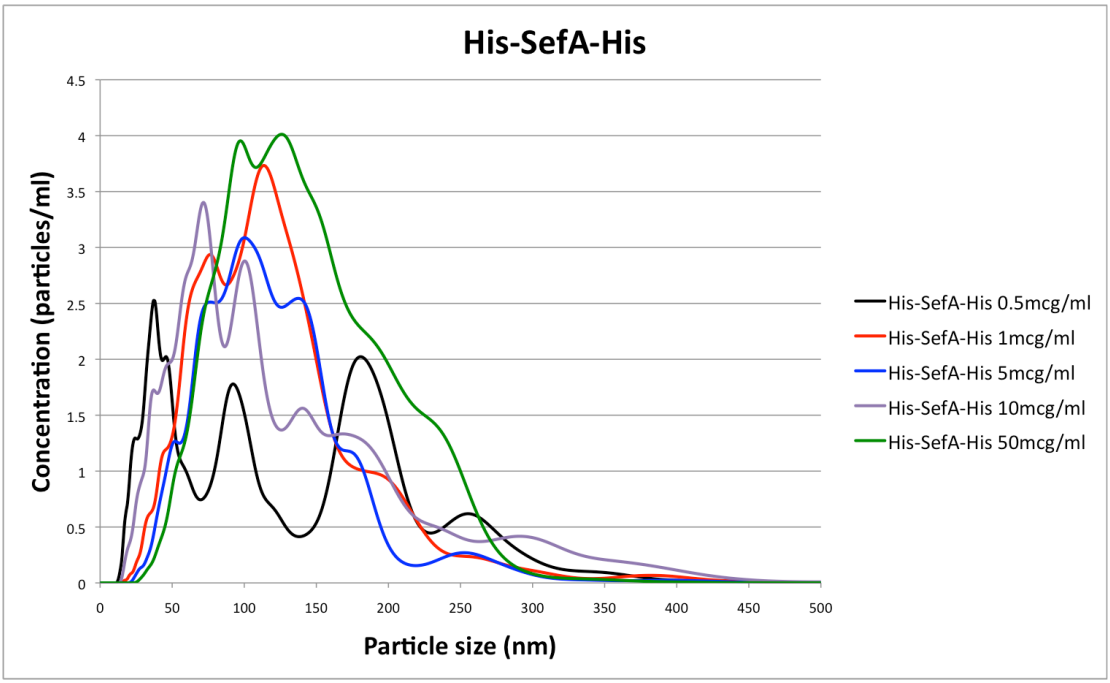

Figure 4.14: Particle size distribution of selenium nanospheres produced in the presence of His-SefA-His in reaction 1.

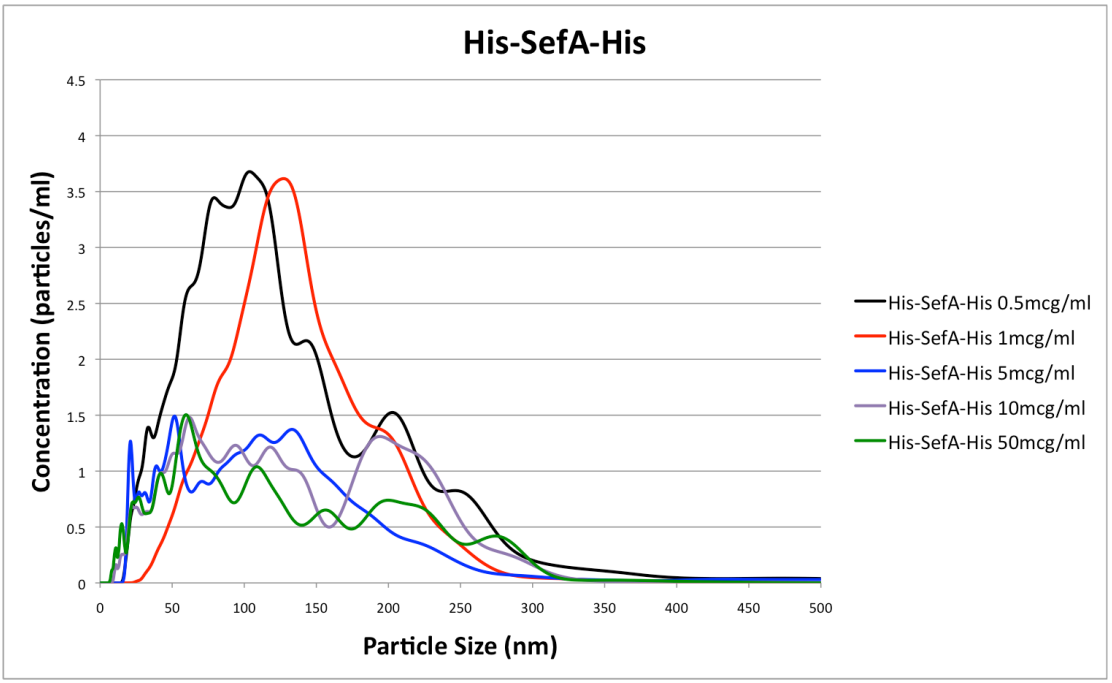

Figure 4.15: Particle size distribution of selenium nanospheres produced in the presence of His-SefA-His in reaction 2.

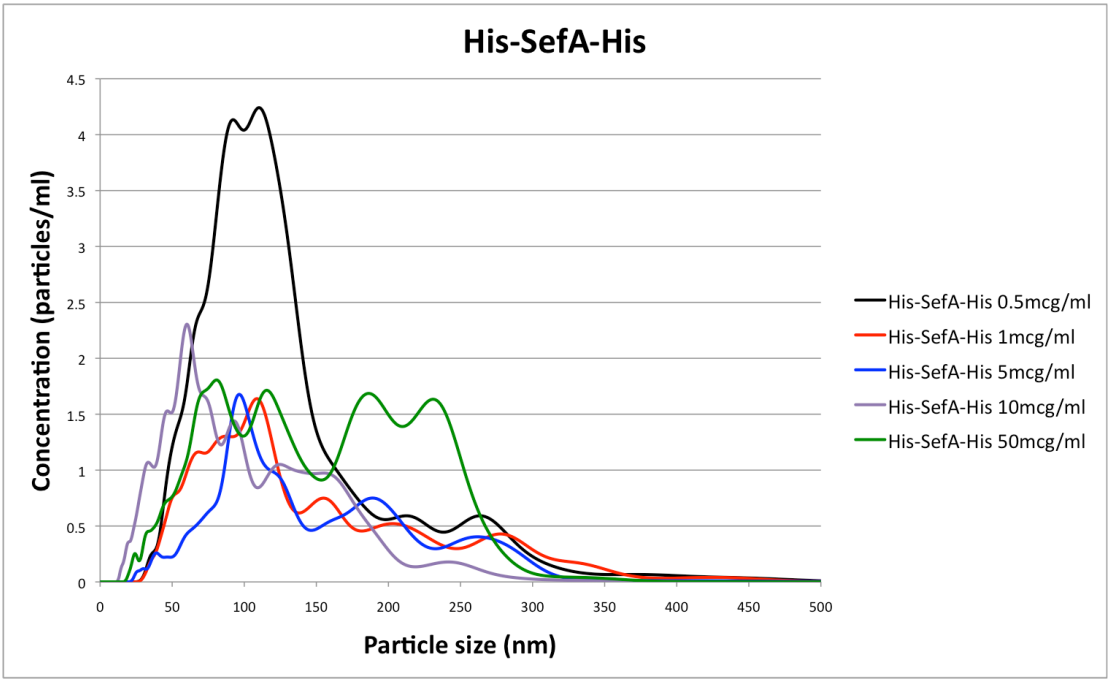

Figure 4.16: Particle size distribution of selenium nanospheres produced in the presence of His-SefA-His in reaction 3.

Figures 4.11, 4.12 and 4.13 show that as the concentration of His-SefA increases, the size distribution of the selenium nanospheres formed decreases. At low concentrations of His-SefA, there is a broad distribution of particle sizes (75 – 175 nm) whereas at higher concentrations the size

distribution of the particles becomes a lot narrower (50 – 100 nm). Figures 4.14 – 4.16 show the size distribution of the nanoparticles produced in the presence of His-SefA-His. No strong trend can be seen here relating size distribution to protein concentration. These plots closely relate to figures 4.17 and 4.18, showing plots of mean particle size against protein concentration for the corresponding protein constructs.

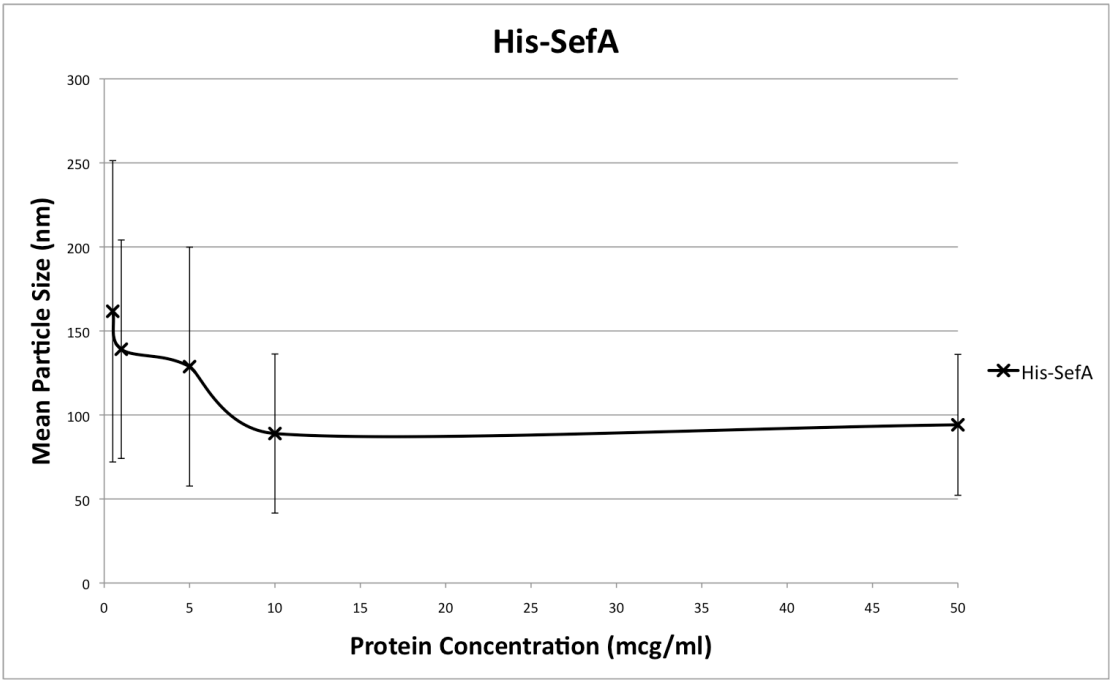

Figure 4.17: A plot of mean particle size at different concentrations of His-SefA.

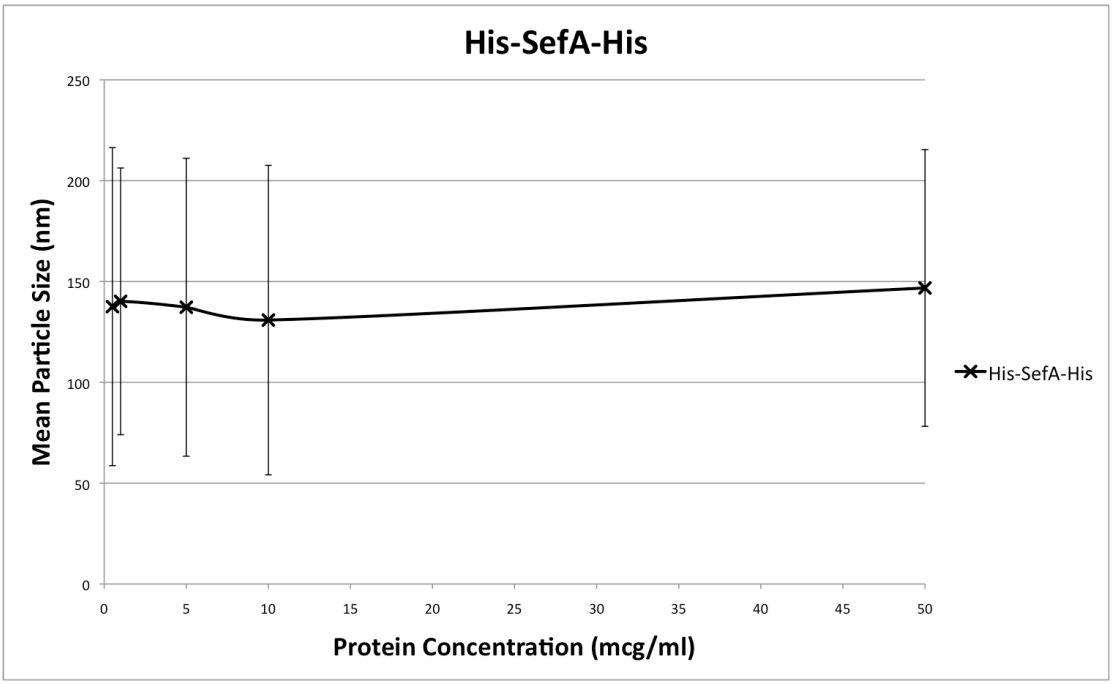

Figure 4.18: A plot of mean particle size at different concentrations of His-SefA-His.

Figure 4.17 shows mean particle size against the concentration of His-SefA, as the concentration of His-SefA increases the mean particle size decreases. It can be seen that as the protein concentration increases the size distribution of the particles decreases. Figure 4.18 shows the same data however for selenium nanoparticles produced in the presence of His-SefA-His. No general trend can be extracted from this plot, increasing the protein concentration does not seem to have an obvious effect on particle size or on size distribution.

4.5 Zeta Potential of His-SefA

The apparent drift velocity of each particle can be recorded using a ZetaSight system. This technology developed by NanoSight Ltd tracks the zeta potential of nanospheres on a particle-by-particle basis. This was applied to those nanospheres produced in the presence of 50 μg/ml of His-SefA. Figure 4.19 shows a plot of zeta potential against particle concentration showing the mean zeta potential to be -39.8 mV.

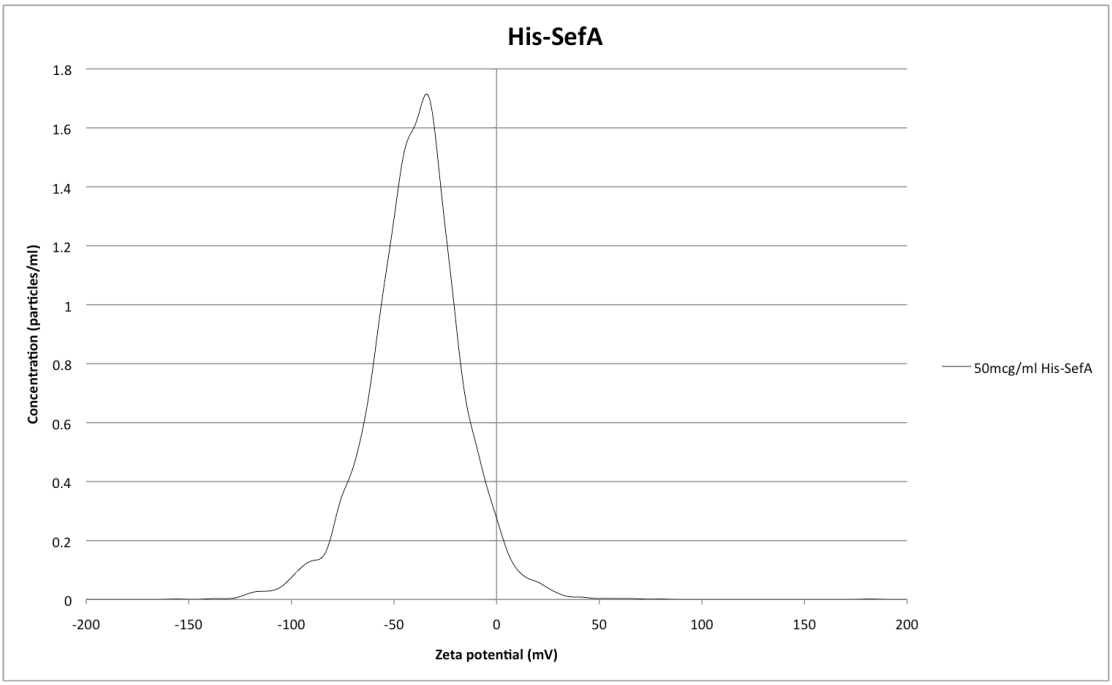

Figure 4.19: A plot of zeta potential against particle concentration.

4.6 Crystallisation Trials for His-SefA-His

Crystallisation trials were run for His-SefA-His (see materials and methods 2.7) and three crystals grew in 0.1 M CAPS buffer (pH 10.5), 1 M NaBr, 40% MPD. The crystals show a rhombus shape and were 1.6 mm in size. It was considered unlikely that they were salt crystals as there was no salt in the growth conditions. These crystals were frozen and then exposed to a high-intensity and finely focussed beam of monochromatic X-ray radiation to produce a diffraction pattern relating to the different properties of the crystal. The crystals did not diffract and so such a diffraction pattern was not produced. To produce crystals that would diffract it would be necessary to optimise crystallisation conditions. The diffraction data collected would need to be of high resolution; at least 2.5 Å.

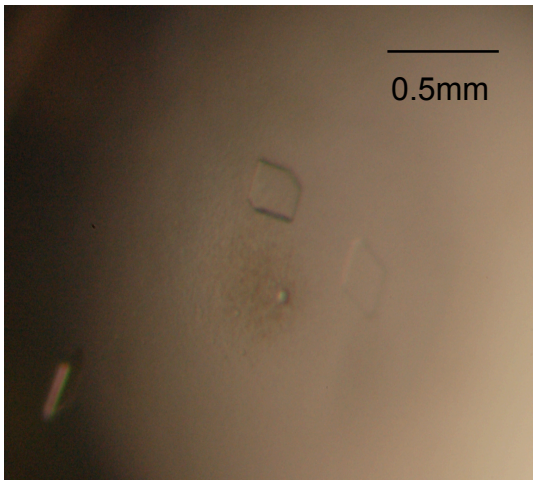

Figure 4.20: Three crystals produced of the His-SefA-His protein.

4.7 Discussion

SDS-PAGE analysis of the expressed and purified His-SefA and His-SefA-His proteins shows that the double His-tagged form of the protein is slightly purer than the mono His-tagged form. There are faint bands apparent at a range of lower molecular weights on the gel, which could indicate the presence of other smaller proteins or could be slight degradation of the SefA proteins. The colour of the selenium particles which are formed as a result of the reaction between reduced GSH and selenite can be seen in the presence of both His-SefA and His-SefA-His respectively. In the presence of each protein it can be seen that an increase in protein concentration results in a decrease in the colour intensity of the protein formed, more dramatically so in the presence of His-SefA. For both reactions absorbance at 400 nm was measured as a function of time, in the presence of His-SefA a general trend can be seen in figure 4.3 that absorbance decreases as protein concentration increases, further confirmed in figure 4.5 where a decrease in final absorbance can be seen as the protein concentration increases. However in the presence of the His-SefA-His protein, there is an increase in absorbance as protein concentration increases from 0.5 μg/ml to 50 μg/ml. An increase in final absorbance with increasing concentration of His-SefA-His confirms this trend.

NTA tracks the nanospheres on a particle-by-particle basis and allows particle size and size distribution to be determined. The plots of particle size against particle concentration for those produced in the presence of His-SefA can be seen, along with similar plots for those produced in the presence of His-SefA-His. For those nanoparticles produced in the presence of the mono His-tagged protein, the size distribution of the nanoparticles becomes much smaller as the protein concentration increases. At 0.5 μg/ml and 1 μg/ml a broad size distribution of the particles can be seen (50 – 200 nm) however at 50 μg/ml this becomes much more narrow (25 – 150 nm). For those selenium particles produced in the presence of His-SefA-His, a similar trend cannot be seen. It would appear that changing the concentration of the protein has no effect on the size distribution of these particles. Looking at a plot of mean particle size against protein concentration, this is further confirmed, as an

increase in protein concentration has no effect on the particle size. For the selenium nanospheres produced in the presence of His-SefA, the mean particle size decreases as protein concentration increases.

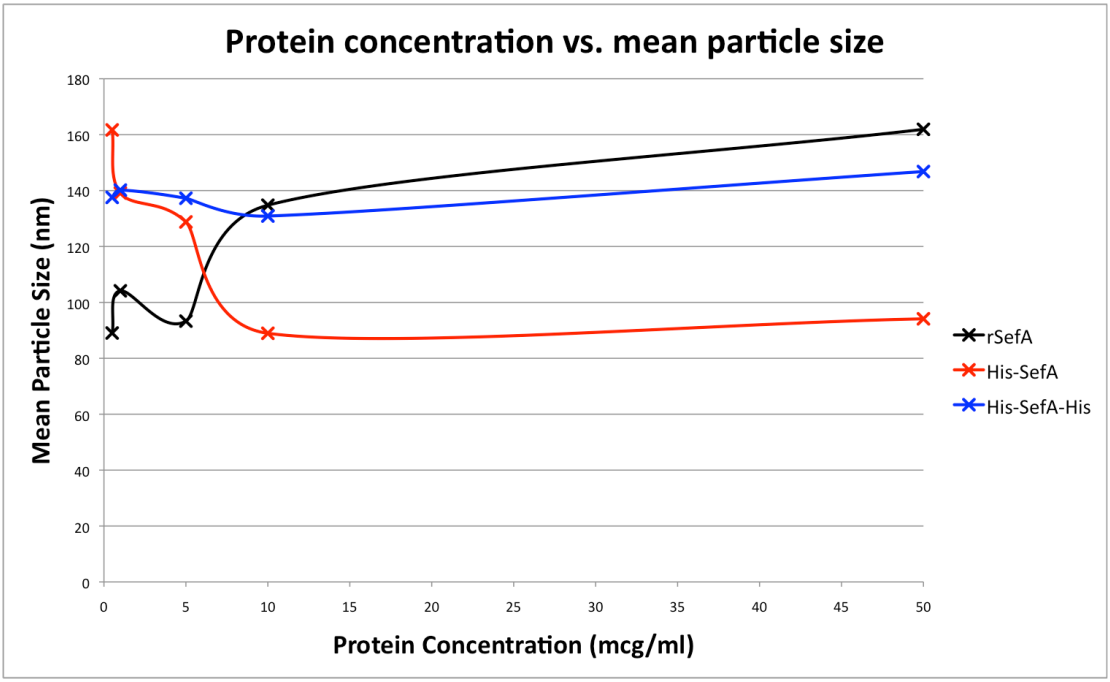

Figure 4.21: An overlay of mean particle size plotted against protein concentration for all three protein constructs; SefA, His-SefA and His-SefA-His.

A plot in figure 4.21 of mean particle size against protein concentration, shows an overlay of all three different forms of the SefA protein: rSefA, His-SefA and His-SefA-His. The formation of selenium nanospheres in the presence of the rSefA protein shows an increase in particle size with increasing protein concentration. The addition of an N-terminal His-tag onto this protein to form His-SefA has the inverse effect and actually shows a decrease in particle size with increasing protein concentration. The addition of a His-tag to the N and C-termini of SefA shows no effect of changing protein concentration on particle size.

The difference in trends across the different protein forms confirms that the addition and removal of His-tags to the SefA protein does have an effect on the properties of the selenium nanospheres formed during the reaction between reduced GSH and selenite. Del Pino *et al.* considered protein adsorption onto nanoparticles as ligand binding (Del Pino *et al.*, 2013). Could the addition of the His-tag onto the protein, before protein adsorption onto the nanoparticle surface, also be considered as ligand binding? The addition of

either an N-terminal or a C-terminal His-tag onto the SefA protein could be having a similar effect to the addition of a ligand and changing the way in which the protein binds around the nanospheres.

It is possible that the His-tag itself is interacting with the selenium particles and this is affecting the way in which they form and their size. Lin and co-workers investigated the effect of protein adsorption on the size of selenium nanoparticles and stated that the amount of protein added to a reaction system will indeed affect the size of the nanoparticles which are formed (Lin *et al.*, 2005). Butler *et al.* suggested that the N-terminus of SefA could be an influencing factor on the way in which SefA folds and assembles (Butler *et al.*, 2012). In this chapter the investigation has focused on the formation of elemental selenium in the presence of SefA forms in which the N-terminus has been blocked by a His-tag. The conservation of this N-terminus could be important for the protein to make protein-protein interactions or protein-nanoparticle interactions.

Peptides have been shown to stabilise nanostructures (Monopoli *et al.*, 2011) and zeta potential analysis of selenium nanospheres produced in the presence of 5 μg/ml His-SefA-His showed a zeta potential of -39.8 mV. Colloidally stable suspensions have a zeta potential of -30 mV or less, destabilised suspensions -15 mV and minimally stable 0 mV (Buchs *et al.*, 2013) (Malvern Instruments Ltd.). This shows that elemental selenium produced in the presence of a protein with two His-tags, one on the N-terminus and one on the C-terminus, are colloidally stable. Abe and co-workers conducted a study investigating apo-ferritin protein nanocages with palladium (Abe *et al.*, 2010). Here it was found that altering the positions of His-residues on the proteins may control the coordination structures of the nanocages. Perhaps the His-tagging affects the protein-particle interactions in such a way that it in fact enhances particle stability.

It was hypothesised that the SefA and selenium may form similar interactions to those between BSA and quantum dots (Bucking *et al.*, 2009). The SefA protein may coat these selenium nanospheres within *T. selenatis* to export them out of the cell. Modifications to the proteins with His-tagging changes the properties of the selenium nanospheres and could therefore be having an effect on the way in which they self-assemble. It is possible that the

addition of a His-tag to the N-terminus or the C-terminus of the protein actually has an effect on how the protein folds and the different structures of these protein forms could then be having different effects on the nanosphere assembly. It is unfortunate that the crystals of the His-SefA-His protein did not diffract as they could have led to discovering the structure of the protein. The lack of effect of His-SefA-His on the size of the selenium nanospheres formed suggests that it is in fact the conservation of the C-terminus of SefA which is important. Perhaps the C-terminus also has an important role in protein-protein interactions and the overall assembly of the SefA-Se nanocage.

5 Concluding comments and future work

5.1 Concluding comments

The work presented here described an investigation of the effect of protein adsorption on selenium nanosphere assembly. This involved looking at three different forms of the selenium export factor protein SefA isolated from *T. selenatis* (Debieux *et al.*, 2011).

Interestingly, very different results regarding the size of nanospheres formed have been seen with each different form of the SefA protein. Selenium nanospheres were produced as a product of the reaction of reduced glutathione and selenite, in the presence of three different forms of SefA. Those produced in the presence of rSefA showed an increase in particle size with increasing protein concentration. By comparison, the reaction was repeated in the presence of the two His-tagged forms of SefA. In the presence of His-SefA, the form with a His-tag only on the N-terminus, particle size decreased as protein concentration increased, however in the presence of the double His-tagged form His-SefA-His, no trend was seen correlating particle size and protein concentration. This confirms the hypothesis that His-tagging a protein does in fact have an effect on the nanoparticles which are formed. The positive correlation between particle size and protein concentration seen when produced in the presence of rSefA, alongside an investigation by Butler *et al.*, (2012), primarily led to the suggestion that the N-terminus of the SefA protein was involved in the nanocage assembly. However the reaction carried out in the presence of His-SefA also showed a correlation, although here particle size was seen to decrease with increasing protein concentration, even though the N-terminus was blocked by a His-tag. It is not yet clear whether the N-terminal region is involved in protein-protein interactions, perhaps with an as yet unidentified protein partner, and therefore influences particle-protein assembly, or if it is the His-tag itself which is interacting with the nanoparticles. The lack of correlation between particle size and protein concentration when analysing the particles produced in the presence of His-SefA-His suggests that perhaps it is not solely the N-terminus which is important for particle assembly. This form of the protein has both the N-

terminus and the C-terminus blocked by His-tags. The absence of a trend here indicates that the C-terminus of SefA plays an important role in how the protein folds and how this protein-nanocage assembles.

These selenium nanoparticles produced *in vitro* are similar to those naturally occurring in the selenate respiring bacterium *T. selenatis*. The form of SefA with no His-tags attached was expected to be the most similar to that found in the bacterium itself. Therefore it was expected that the selenium nanospheres produced in the presence of this protein would be the most similar to those produced within the bacterium. The selenium nanospheres isolated from *T. selenatis* were approximately 130 nm in size, nanoparticles of 130 nm in size were produced *in vitro* in the presence of 10 μg/ml SefA. This suggests that the internal concentration of SefA within *T. selenatis*, at the point of selenium nanosphere formation, could be in the order of 10 μg/ml. Although the nanoparticles formed at 10 μg/ml SefA were 130 nm in size, a broader range of sizes was seen across the full range of protein concentrations (0.5 μg/ml – 50 μg/ml). This indicates there could be another influencing factor within *T. selenatis*, this could be another peptide which is interacting with SefA and having an effect on particle formation.

5.2 Future work

To carry on with the work outlined in this study, the isolation of a construct of SefA with a His-tag only on the C-terminus (SefA-His) could give more information on the need for conservation of the C-terminus of SefA. The N-terminus of His-SefA-His could be cleaved to form SefA-His however separating a His-tag from the resulting His-tagged protein SefA-His could be a problem. A data set including a protein with the C-terminus blocked, but not the N-terminus could give an insight into whether the N- or C-termini are influential in protein-selenium interactions and the assembly of the nanocage.

This work has suggested that there could be another protein in *T. selenatis* which is interacting with SefA and could be influencing the way in which these nanospheres are formed within the cell. The possibility of there being a partner protein to SefA could affect the way in which SefA interacts with the selenium and forms a nanocage around it. Identification of any other

interacting proteins within *T. selenatis* could give further insight as to how the selenium nanospheres are exported out of the cell, perhaps SefA is not the only influencing factor.

Debieux and co-workers obtained electron microscopy images of selenium nanospheres produced within *T. selenatis* at different stages of the growth phases (Debieux *et al.*, 2011). It would be beneficial to obtain some similar images for the nanoparticles produced *in vitro* to compare the shape as this might indicate how the different proteins are interacting with the nanospheres. It would also be advantageous to carry on with crystallisation trials for the SefA protein. To obtain the protein's structure could give a lot more information on the potential for interactions between proteins and between the protein and the nanospheres.

6 References

Abe, S., Hikage, T., Watanabe, Y., Kitagawa, S. and Ueno, T. (2010). "Mechanism of accumulation and incorporation of organometallic Pd complexes into the protein nanocage of apo-ferritin." Inorg Chem **49**(15): 6967-6973.

Agapakis, C. M., Boyle, P. M. and Silver, P. A. (2012). "Natural strategies for the spatial optimization of metabolism in synthetic biology." Nature Chemical Biology **8**(6): 527-535.

Almeida, A. J. and Souto E. (2007). "Solid lipid nanoparticles as a drug delivery system for peptides and proteins." Advanced Drug Delivery Reviews **59**(6): 478-490.

Arner, E. S. J. (2012). “History of Selenium Research.” Selenium: Its Molecular Biology and Role in Human Health, Third Edition 1-19.

Baron, M. H., Revault, M., Servagent-Noinville, S., Abadie, J. and Quiquampoix, H. (1999). "Chymotrypsin Adsorption on Montmorillonite: Enzymatic Activity and Kinetic FTIR Structural Analysis." Journal of Colloid and Interface Science **214**(2): 319-332.

Brandes, N., Welzel, P. B., Werner, C. and Kroh, L. W. (2006). "Adsorption-induced conformational changes of proteins onto ceramic particles: Differential scanning calorimetry and FTIR analysis." Journal of Colloid and Interface Science **299**(1): 56-69.

Buchs, B., Evangelou, M. W. H., Winkel, L., H., E. and Lenz, M. (2013). "Colloidal Properties of Nanoparticular Biogenic Selenium Govern Environmental Fate and Bioremediation Effectiveness." Environmental Science & Technology **47**(5): 2401-2407.

Buecking, W., Massadeh, S., Merkulov, A., Xu, S. and Nann, T. (2010). "Electrophoretic properties of BSA-coated quantum dots." Analytical and Bioanalytical Chemistry **396**(3): 1087-1094.

Butler, C. S. (2012). The complexity of bacterial selenate respiration: Metals, non-metals and minerals. The Biochemist **34**(5): 23-27.

Butler, C. S., Debieux, C., M., Dridge, E., J., Splatt, P. and Wright, M. (2012). "Biomineralization of selenium by the selenate-respiring bacterium *Thauera selenatis*." Biochemical Society transactions **40**(6): 1239-1243.

Chang, J.-S., Chang, K., L., Hwang, D., F. and Kong, Z., L. (2007). "In Vitro Cytotoxicitiy of Silica Nanoparticles at High Concentrations Strongly Depends on the Metabolic Activity Type of the Cell Line." Environmental Science & Technology **41**(6): 2064-2068.

Coppage, R., Slocik, J., M., Briggs, B., D., Frenkel, A., I., Heinz, H., Naik, R., R. and Knecht, M., R. (2011). "Crystallographic Recognition Controls Peptide Binding for Bio-Based Nanomaterials." Journal of the American Chemical Society **133**(32): 12346-12349.

Debieux, C. M., Dridge, E., J., Mueller, C., M., Splatt, P., Paszkiewicz, K., Knight, I., Florance, H., Love, J., Titbull, R., W., Lewis, R., J., Richardson, D., J. and Butler, C., S. (2011). "A bacterial process for selenium nanosphere assembly." Proceedings of the National Academy of Sciences of the United States of America **108**(33): 13480-13485.

Delepelaire, P. (2004). "Type I secretion in gram-negative bacteria." Biochimica et Biophysica Acta (BBA) - Molecular Cell Research **1694**(1–3): 149-161.

Dell'orco, D., Lundqvist, M., Cedervall, T. and Linse, S. (2012). "Delivery success rate of engineered nanoparticles in the presence of the protein corona: a systems-level screening." Nanomedicine : nanotechnology, biology, and medicine **8**(8).

DeMoll-Decker, H. and Macy, J. (1993). "The periplasmic nitrite reductase of Thauera selenatis may catalyze the reduction of selenite to elemental selenium." Archives of Microbiology **160**(3): 241-247.

Derfus, A. M., Chan, W., C., W. and Bhatia, S., N. (2003). "Probing the Cytotoxicity of Semiconductor Quantum Dots." Nano Letters **4**(1): 11-18.

Dittrich, C., Burckhardt, C., J. and Danuser, G. (2012). "Delivery of membrane impermeable cargo into CHO cells by peptide nanoparticles targeted by a protein corona." Biomaterials **33**(9): 2746-2753.

Dobias, J., Suvorova, E., I. and Bernier-Latmani, R. (2011). "Role of proteins in controlling selenium nanoparticle size." Nanotechnology **22**(19).

Dombu, C. Y. and Betbeder, D. (2013). "Airway delivery of peptides and proteins using nanoparticles." Biomaterials **34**(2).

Dridge, E. J., Watts, C., A., Jepson, B., J., Line, K., Santini, J., M., Richardson, D., J. and Butler, C., S. (2007). "Investigation of the redox centres of periplasmic selenate reductase from Thauera selenatis by EPR spectroscopy." Biochem J **408**(1): 19-28.

Dungan, R. S., Yates, S., R. and Frankenberger, W., T., Jr. (2003). "Transformations of selenate and selenite by Stenotrophomonas maltophilia isolated from a seleniferous agricultural drainage pond sediment." Environmental Microbiology **5**(4): 287-295.

Ehrenberg, M. S., Friedman, A., E., Finkelstein, J., N., Oberdorster, G. and McGrath, J., L. (2009). "The influence of protein adsorption on nanoparticle association with cultured endothelial cells." Biomaterials **30**(4): 603-610.

Emerson, D., Fleming, E., J. and McBeth, J., M. (2010). Iron-Oxidizing Bacteria: An Environmental and Genomic Perspective. Annual Review of Microbiology, Vol 64, 2010. S. Gottesman and C. S. Harwood. **64:** 561-583.

Fatisson, J., Quevedo, I., R., Wilkinson, K., J. and Tufenkji, N. (2012). "Physicochemical characterization of engineered nanoparticles under physiological conditions: Effect of culture media components and particle surface coating." Colloids and Surfaces B-Biointerfaces **91**: 198-204.

Fletcher, J. M., Harniman, R., L., Barnes, F., R., Boyle, A., L., Collins, A., Mantell, J., Sharp, T., H., Antognozzi, M., Booth, P., J., Linden, N., Miles, M., J., Sessions, R., B., Verkade, P. and Woolfson, D., N. (2013). "Self-Assembling Cages from Coiled-Coil Peptide Modules." Science **340**(6132): 595-599.

Ganther, H. E. (1971). "Reduction of selenotrisulfide derivative of glutathione to a persulfide analog by glutathione reductase." Biochemistry **10**(22): 4089-4098.

Gebauer, J. S., Malissek, M., Simon, S., Knauer, S., K., Maskos, M., Stauber, R., H., Peukert, W. and Treuel, L. (2012). "Impact of the Nanoparticle–Protein Corona on Colloidal Stability and Protein Structure." Langmuir **28**(25): 9673-9679.

Gerrard, T. L., Telford, J., N. and Williams, H., H. (1974). "Detection of selenium deposits in *Escherichia-coli* by electron microscopy." Journal of Bacteriology **119**(3): 1057-1060.

Ghosh, A., Mohod, A., M., Paknikar, K., M. and Jain, R., K. (2008). "Isolation and characterization of selenite- and selenate-tolerant microorganisms from selenium-contaminated sites." World Journal of Microbiology and Biotechnology **24**(8): 1607-1611.

Hammer, D. A. and Kamat, N. P. (2012). "Towards an artificial cell." FEBS Letters **586**(18): 2882-2890.

Hashimoto, H., Yokoyama, S., Asaoka, H., Kusano, Y., Ikeda, Y., Seno, M., Takada, J., Fujii, T., Nakanishi, M. and Murakami, R. (2007). "Characteristics of hollow microtubes consisting of amorphous iron oxide nanoparticles produced by iron oxidizing bacteria, Leptothrix ochracea." Journal of Magnetism and Magnetic Materials **310**(2): 2405-2407.

Hashimoto, H., Fujii, T., Kohara, S., Asaoka, H., Kusano, Y., Ikeda, Y., Nakanishi, M., Benino, Y., Nanba, T. and Takada, J. (2012). "Amorphous structure of iron oxide of bacterial origin." Materials Chemistry and Physics **137**(2): 571-575.

Hauck, T. S., Ghazani, A., A. and Chan, W., C. (2008). "Assessing the Effect of Surface Chemistry on Gold Nanorod Uptake, Toxicity, and Gene Expression in Mammalian Cells." Small **4**(1): 153-159.

Heider, J. and Bock, A. (1993). "Selenium metabolism in micro-organisms." Advances in Microbial Physiology, Vol 35 **35**: 71-109.

Hoshino, A., Fujioka, K., Oku, T., Suga, M., Sasaki, Y., F., Ohta, T., Yasuhara, M., Suzuki, K. and Yamamoto, K. (2004). "Physicochemical Properties and Cellular Toxicity of Nanocrystal Quantum Dots Depend on Their Surface Modification." Nano Letters **4**(11): 2163-2169.

Hu, W., Peng, C., Lv, M., Li, X., Zhang, Y., Chen, N., Fan, C. and Huang, Q. (2011). "Protein Corona-Mediated Mitigation of Cytotoxicity of Graphene Oxide." ACS Nano **5**(5): 3693-3700.

Ike, M., Takahashi, K., Fujita, T., Kashiwa, M. and Fujita, M. (2000). "Selenate reduction by bacteria isolated from aquatic environment free from selenium contamination." Water Research **34**(11): 3019-3025.

Illum, L. (2007). "Nanoparticulate systems for nasal delivery of drugs: A real improvement over simple systems?" Journal of Pharmaceutical Sciences **96**(3): 473-483.

Jeong, Y.-K., Sohn, Y. and Kang, J., G. (2014). "Synthesis and characterization of Eu(III)-incorporated silica nanoparticles for application to UV-LED." Journal of Colloid and Interface Science **423**(0): 41-47.

Johnson, J. A., Saboungi, M-L., Thiyagarajan, P., Csencsits, R. and Meisel, D. (1998). "Selenium Nanoparticles: A Small-Angle Neutron Scattering Study." The Journal of Physical Chemistry B **103**(1): 59-63.

Kessi, J. and Hanselmann, K. W. (2004). "Similarities between the abiotic reduction of selenite with glutathione and the dissimilatory reaction mediated by *Rhodospirillum rubrum* and *Escherichia coli*." Journal of Biological Chemistry **279**(49): 50662-50669.

Klein, J. (2007). "Probing the interactions of proteins and nanoparticles." Proceedings of the National Academy of Sciences **104**(7): 2029-2030.

Krafft, T., Bowen, A., Theis, F. and Macy, J., M. (2000). "Cloning and sequencing of the genes encoding the periplasmic-cytochrome B-containing selenate reductase of Thauera selenatis." DNA sequence : the journal of DNA sequencing and mapping **10**(6): 365-377.

Kreuter, J., Nanoparticles as drug delivery systems, in: H.S. Nalwa (Ed.), Encyclopedia of Nanoscience and Nanotechnology, vol. 7, American Scientific Publishers, Stevenson Ranch, U.S.A., 2004, pp. 161–180.

Kurakhmaeva, K. B., Djindjikhashvili, I., A., Petrov, V., E., Balabanyan, V., U., Voronina, T., A., Trofimov, S., S., Kreuter, J., Gelperina, S., Begley, D. and Alyautdin, R., N. (2009). "Brain targeting of nerve growth factor using poly(butyl cyanoacrylate) nanoparticles." J Drug Target **17**(8): 564-574.

Lee, J.-H., Han, J., Choi, H. and Hur, H., G. (2007). "Effects of temperature and dissolved oxygen on Se(IV) removal and Se(0) precipitation by Shewanella sp. HN-41." Chemosphere **68**(10): 1898-1905.

Lin, Z.-H. and Wang, C. R. (2005). "Evidence on the size-dependent absorption spectral evolution of selenium nanoparticles." Materials Chemistry and Physics **92**(2–3): 591-594.

Lloyd, J. R. (2003). "Microbial reduction of metals and radionuclides." FEMS Microbiology Reviews **27**(2–3): 411-425.

Losi, M. E. and Frankenberger, W. T. (1997). "Reduction of selenium oxyanions by *Enterobacter cloacae* SLD1a-1: Isolation and growth of the bacterium and its expulsion of selenium particles." Applied and Environmental Microbiology **63**(8): 3079-3084.

Lowe, E. C., Watts, C., A., Richardson, D., G., Santini, J., M., Singleton, I. and Butler, C., S. (2006). "The bioenergetics of selenate respiration in *Thauera selenatis*." Biochimica Et Biophysica Acta-Bioenergetics: 203-203.

Lowe, E. C., Bydder, S., Hartshorne, R., S., Tape, H., L., Dridge, E., J., Debieux, C., M., Paszkiewicz, K., Singleton, I., Lewis, R., J., Santini, J., M., Richardson, D., J. and Butler, C., S. (2010). "Quinol-cytochrome c Oxidoreductase and Cytochrome c4 Mediate Electron Transfer during Selenate Respiration in Thauera selenatis." Journal of Biological Chemistry **285**(24): 18433-18442.

Lynch, I., Dawson, K., A. and Linse, S. (2006). "Detecting Cryptic Epitopes Created by Nanoparticles." Sci. STKE **2006**(327): pe14-.

Macy, J. M., Michel, T., A. and Kirsch, D., G. (1989). "Selenate reduction by a Pseudomonas species: a new mode of anaerobic respiration." FEMS microbiology letters **52**(1-2): 195-198.

Macy, J. M., Rech, S., Auling, G., Dorsch, M., Stackebrandt, E. and Sly, L., I. (1993). "*Thauera-Selenatis* Gen-Nov, Sp-Nov, a member of the beta-subclass of proteobacteria with a novel type of anaerobic respiration." International Journal of Systematic Bacteriology **43**(1): 135-142.

Malvern Instruments Ltd.: Worcester, UK, 2004; ZetaSizer Nano Series User Manual Version 2.1;
http://nbct.cornell.edu/facilities/downloads/Zetasizer%20Manual.pdf

Millington, K. R., Osmond, M., J. and McCall, M., J. (2014). "Detecting free radicals in sunscreens exposed to UVA radiation using chemiluminescence." Journal of Photochemistry and Photobiology B: Biology **133**(0): 27-38.

Monopoli, M. P., Walczyk, D., Campbell, A., Elia, G., Lynch, I., Baldelli Bombelli, F. and Dawson, K., A. (2011). "Physical-Chemical Aspects of Protein Corona: Relevance to in Vitro and in Vivo Biological Impacts of Nanoparticles." Journal of the American Chemical Society **133**(8): 2525-2534.

Narasingarao, P. and Häggblom, M. M. (2007). "Identification of Anaerobic Selenate-Respiring Bacteria from Aquatic Sediments." Applied and Environmental Microbiology **73**(11): 3519-3527.

Nel, A. E., Madler, L., Velegol, D., Xia, T., Hoek, E., M., V., Somasundaran, P., Klaessig, F., Castranova, V. and Thompson, M. (2009). "Understanding biophysicochemical interactions at the nano-bio interface." Nature Materials **8**(7): 543-557.

Nemmar, A., Hoet, P., H., Vanquickenborne, B., Dinsdale, D., Thomeer, M., Hoylaerts, M., F., Vanbilloen, H., Mortelmans, L. and Nemery, B. (2002). "Passage of inhaled particles into the blood circulation in humans." Circulation **105**(4): 411-414.

Ogasawara, Y., Lacourciere, G. and Stadtman, G., C. (2001). "Formation of a selenium-substituted rhodanese by reaction with selenite and glutathione:

Possible role of a protein perselenide in a selenium delivery system." Proceedings of the National Academy of Sciences of the United States of America **98**(17): 9494-9498.

Oremland, R. S., Herbel, M., J., Switzer Blum, J., Langley, S., Beveridge, T., J., Ajayan, P., M., Sutto, T., Ellis, A., V. and Curran, S. (2004). "Structural and spectral features of selenium nanospheres produced by se-respiring bacteria." Applied and Environmental Microbiology **70**(1): 52-60.

Painter, E. P. (1941). "The chemistry and toxicity of selenium compounds, with special reference to the selenium problem." Chemical Reviews **28**(2): 179-213.

Pino, P. d., Pelaz, B., Zhang, Q., Maffre, P., Ulrich Nienhaus, G. and Parak, W., J. (2014). "Protein corona formation around nanoparticles - from the past to the future." Materials Horizons **1**(3): 301-313.

Prakash, N. T., Sharma, N., Prakash, R., Raina, K., K., Fellowes, J., Pearce, C., I., Lloyd, J., R. and Pattrick, R., A., D. (2009). "Aerobic microbial manufacture of nanoscale selenium: exploiting nature's bio-nanomineralization potential." Biotechnology Letters **31**(12): 1857-1862.

Prapainop, K., Witter, D., P. and Wentworth, P., Jr. (2012). "A Chemical Approach for Cell-Specific Targeting of Nanomaterials: Small-Molecule-Initiated Misfolding of Nanoparticle Corona Proteins." Journal of the American Chemical Society **134**(9): 4100-4103.

Prieur, E., Betbeder, D., Niedergang, F., Major, M., Alcover, A., Davignon, J., L. and Davrinche, C. (1996). "Combination of human cytomegalovirus recombinant immediate-early protein (IE1) with 80 nm cationic biovectors: protection from proteolysis and potentiation of presentation to CD4+ T-cell clones in vitro." Vaccine **14**(6): 511-520.

Richardson, D. J. (2000). "Bacterial respiration: a flexible process for a changing environment." Microbiology-Uk **146**: 551-571.

Saiki, M. and Lowe, T. P. (1987). "Selenium in aquatic organisms from subsurface agricultural drainage water, San Joaquin Valley, California." Archives of Environmental Contamination and Toxicology **16**(6): 657-670.

Sander, C. S., Chang, H., Salzmann, S., Muller, C., S., Ekanayake-Mudiyanselage, S., Elsner, P. and Thiele, J., J. (2002). "Photoaging is associated with protein oxidation in human skin in vivo." Journal of Investigative Dermatology **118**(4): 618-625.

Saptarshi, S., R., Duschl, A. and Lopata, A., L. (2013). "Interaction of nanoparticles with proteins: relation to bio-reactivity of the nanoparticle." Journal of Nanobiotechnology **11**(1): 26.

Schroder, I., Rech, S., Krafft, T. and Macy, J., M. (1997). "Purification and characterization of the selenate reductase from *Thauera selenatis*." Journal of Biological Chemistry **272**(38): 23765-23768.

Soon-Bark, K. and Ken Won, L. (2004). Aerosol Nanoparticles. Dekker Encyclopedia of Nanoscience and Nanotechnology - Six Volume Set (Print Version), CRC Press.

Spring, S. (2006). The Genera Leptothrix and Sphaerotilus. The Prokaryotes. M. Dworkin, S. Falkow, E. Rosenberg, K.-H. Schleifer and E. Stackebrandt, Springer New York**:** 758-777.

Suwa, Y., Sumino, T. and Noto, K. (1997). "Phylogenetic relationships of activated sludge isolates of ammonia oxidizers with different sensitivities to ammonium sulfate." The Journal of General and Applied Microbiology **43**(6): 373-379.

Takada, J.; Fujii, T.; Nakanishi, M. Japan patent Tokkai JP 2008−177061 (2008). The potential as a cathode material was publicized in the form of patent.

Tan, M. L., Choong, P., F. and Dass, C., R. (2010). "Recent developments in liposomes, microparticles and nanoparticles for protein and peptide drug delivery." Peptides **31**(1): 184-193.

Tanaka, S., Kerfeld, C., A., Sawaya, M., R., Cai, F., Heinhorst, S., Cannon, G., C. and Yeates, T., O. (2008). "Atomic-level models of the bacterial carboxysome shell." Science **319**(5866): 1083-1086.

Tomei, F. A., Barton, L., L., Lemanski, C., L., Zocco, T., G., Fink, N., H. and Sillerud, L., O. (1995). "Transformation of selenate and selenite to elemental selenium by *Desulfovibrio-desulfuricans*." Journal of Industrial Microbiology **14**(3-4): 329-336.

Treuel, L., Brandholt, S., Maffre, P., Wiegele, S., Shang, L. and Ulrich Nienhaus, G. (2013). "Impact of Protein Modification on the Protein Corona on Nanoparticles and Nanoparticle–Cell Interactions." ACS Nano **8**(1): 503-513.

Uchida, M., Klem, M., T., Allen, M., Suci, P., Flenniken, M., Gillitzer, E., Varpness, Z., Liepold, L., O., Young, M. and Douglas, T. (2007). "Biological containers: Protein cages as multifunctional nanoplatforms." Advanced Materials **19**(8): 1025-1042.

Wohlfart, S., Gelperina, S. and Kreuter, J. (2012). "Transport of drugs across the blood-brain barrier by nanoparticles." J Control Release **161**(2): 264-273.

Wolfram, J., Yang, Y., Shen, J., Moten, A., Chen, C., Shen, H., Ferrari, M. and Zhao, Y. (2014). "The nano-plasma interface: Implications of the protein corona." Colloids and Surfaces B: Biointerfaces http://dx.doi.org/10.1016/j.colsurfb.2014.02.035

Yang, F., Tang, Q., Zhong, X., Bai, Y., Chen, T., Zhang, Y., Li, Y. and Zheng, W. (2012). "Surface decoration by *Spirulina* polysaccharide enhances the cellular uptake and anticancer efficacy of selenium nanoparticles." International Journal of Nanomedicine **7**: 835-844.

Zhang J.S., P.R.O.C. Patent 97107038.5, June 17, 1998

Zhang, L., Li, D. and Gao, P. (2012). "Expulsion of selenium/protein nanoparticles through vesicle-like structures by *Saccharomyces cerevisiae* under microaerophilic environment." World journal of microbiology & biotechnology **28**(12).

Zhang S.Y., P.R.O.C. Patent 02138643.9, May 7, 2003.